Title

Convective overshooting and penetration in a Boussinesq spherical shell

Journal

Monthly Notices of the Royal Astronomical Society, 484(1)

ISSN

0035-8711

Authors

Korre, L
Garaud, P
Brummell, NH

Publication Date

2019-03-21

DOI

10.1093/mnras/stz047

Peer reviewed

Monthly Notices
of the
ROYAL ASTRONOMICAL SOCIETY

MNRAS **484,** 1220–1237 (2019)
Advance Access publication 2019 January 07

doi:10.1093/mnras/stz047

Convective overshooting and penetration in a Boussinesq spherical shell

L. Korre,* P. Garaud* and N.H. Brummell*

Department of Applied Mathematics, Jack Baskin School of Engineering, University of California Santa Cruz, 1156 High Street, Santa Cruz, CA 95064, USA

Accepted 2019 January 3. Received 2018 December 6; in original form 2018 July 20

ABSTRACT

We study the dynamics associated with the extension of turbulent convective motions from a convection zone (CZ) into a stable region (RZ) that lies below the latter. For that purpose, we have run a series of 3D direct numerical simulations solving the Navier–Stokes equations under the Boussinesq approximation in a spherical shell geometry. We observe that the overshooting of the turbulent motions into the stably stratified region depends on three different parameters: the relative stability of the RZ, the transition width between the two, and the intensity of the turbulence. In the cases studied, these motions manage to partially alter the thermal stratification and induce thermal mixing, but not so efficiently as to extend the nominal CZ further down into the stable region. We find that the kinetic energy below the convection zone can be modelled by a half-Gaussian profile whose amplitude and width can be predicted a priori for all of our simulations. We examine different dynamical length-scales related to the depth of the extension of the motions into the RZ, and we find that they all scale remarkably well with a length-scale that stems from a simple energetic argument. We discuss the implications of our findings for 1D stellar evolution calculations.

Key words: convection – Sun: interior – stars: interiors.

1 INTRODUCTION

Understanding the dynamical interaction between an unstable turbulent convective region and an adjacent stable one remains a long-standing unsolved problem in fluid dynamics. This situation is nevertheless fairly ubiquitous in both geophysical and astrophysical settings. Here on Earth for example, it commonly occurs in the atmosphere, where re-radiance of solar surface warming creates a mixed layer below the very stable nocturnal inversion layer (Deardorff, Willis & Lilly 1969). In stars, which are the main topic of this paper, the coexistence of convective and radiative layers is almost ubiquitous across masses and evolutionary stages. For example, A-type stars possess two convection zones, an upper one driven predominantly by the ionization of hydrogen and a lower one driven by the second ionization of helium, with a radiative zone in between. In the Sun, by contrast, an outer convection zone sits atop an inner radiative zone and below a stable atmosphere, and the transitions are due to changes in the heat capacity (caused by the partial ionization zones of hydrogen and helium) and opacity (due to the temperature dependence of heavier ions). Since there is no impermeable interface between the stable and unstable layers, fluid flows originating from one can continue into the other. Primary questions are then whether the convective region can be extended from its original size, and whether the stability characteristics of the system are altered significantly. In all that follows, we shall adopt the terminology introduced by Zahn (1991): if motions are found beyond the convective layer but do not extend its size then the dynamics are termed 'overshooting'; if the convective region is extended, the dynamics are called 'penetration'.

Any form of mixing beyond the classical boundary set by the Schwarzschild criterion could have crucial impacts on stellar evolution and surface abundances through the transport of chemicals and angular momentum (e.g. Straus, Blake & Schramm 1976; Spite & Spite 1982; Ahrens, Stix & Thorn 1992; Pinsonneault 1997; Herwig 2000; Baraffe et al. 2017). The transport of magnetic fields between the two regions has also been suggested as playing a major role in the dynamo process (e.g. van Ballegooijen 1982; Parker 1993; Charbonneau & MacGregor 1997). Furthermore, thanks to the development of helio- and asteroseismology, we now have the opportunity to directly measure the extent of an adiabatically stratified zone (e.g. Christensen-Dalsgaard, Gough & Thompson 1991; Silva Aguirre et al. 2011). This provides a direct test of stellar evolution, and can, in particular, reveal the presence of penetration beyond the expected edge of a convective region (e.g. Deheuvels et al. 2016; Christensen-Dalsgaard, Gough & Knudstrup 2018). Because of its obvious importance, a great body of work has already been generated on penetrative and overshooting convection, and yet some of the crucial questions remain poorly understood. In what follows, we summarize some of the salient modelling milestones of the field, review any outstanding questions, and place our work in their context.

* E-mail: lkorre@ucsc.edu (LK); pgaraud@soe.ucsc.edu (PG); brummell@soe.ucsc.edu (NHB)

The answer to the most basic question of 'does penetration or overshooting actually happen?' has been addressed using a classic example of such dynamics, the ice–water system. Adjacent convective and stable regions in this system can be created thanks to the unusual equation of state for water, which is quadratic with a density maximum at 4 °C. When a layer of water sits on top of ice (at 0 °C) with an upper boundary temperature of more than 4 °C, a system is created where a convectively unstable layer (between the ice and the location of the density maximum) sits below a convectively stable layer (above the density maximum). A long history of exploration of this problem exists, from experiments (e.g. Malkus 1960; Townsend 1964), through linear and weakly non-linear analytic work (e.g. Veronis 1963), to numerical simulations both old (e.g. Musman 1968; Moore & Weiss 1973) and new (e.g. Couston et al. 2017). This simple toy model clearly demonstrates that the weak overshooting predicted by linear theory is replaced by deeper penetration when non-linear feedback on the thermal stratification is allowed. This raises the crucial question of whether similarly large deviations from linear theory predictions (the Schwarzschild criterion) exist in stars.

Answering this question requires moving beyond the assumptions of the works cited above, which was almost all 2D and (essentially) incompressible. A first attempt to understand 3D and compressible effects numerically came from modelling via modal expansions, an approach that is motivated by the observable cellular nature of convection. The horizontal structure of the flow is expanded as a low-order discrete spectrum of horizontal planform modes, allowing numerical resources to be devoted to solving the vertical and temporal problem. This approach, first introduced by Herring (1963) and Roberts (1966), but popularized in a series of papers by Gough, Spiegel and Toomre (Gough, Spiegel & Toomre 1975; Toomre, Gough & Spiegel 1977, 1982), was first applied to the Bénard convection problem, and commonly uses severe truncations of the modal expansion (1–3 modes) with planforms such as rolls, squares, and hexagons.

The technique has been extended to penetrative and overshooting problems involving multiple layers in a number of ways. Using a complex equation of state to include the ionization regions, as well as the anelastic formalism, the papers by Latour et al. (Latour et al. 1976; Toomre et al. 1976; Latour, Toomre & Zahn 1981) study the convection zones of A-type stars and find that they could interact despite the intervening radiative zone thanks to extended fluid motions. Somewhat later, Zahn, Toomre & Latour (1982) and Massaguer et al. (1984) simplified the model set-up to address the question of penetration specifically. Using Boussinesq and anelastic equations, respectively, they initiate layers by directly specifying a depth-dependent background adiabatic gradient in order to study a single convection zone sandwiched between two stable layers. This compact series of papers has led to some important realizations. First, a fairly deep penetration of the order of the depth of the unstable layer is found in all cases that agrees well with laboratory experiments (although it depends on the stability of the stable layer and on the aspect ratio of the cells). Secondly, flow asymmetries make substantial differences in the amount of overshoot or penetration. For instance, stratification combined with pressure effects (buoyancy braking in the upflows and enhanced driving in the downflows) in the anelastic case causes slower upflows and faster downflows compared to the Boussinesq case, which leads to enhanced downward penetration. Topological asymmetries (as induced by non-Cartesian effects or simply through a particular selection of horizontal planform) have similarly important impact on the problem.

The discovery of the importance of flow asymmetries on the extent of overshooting and penetration has naturally prompted new investigations into the effect of compressibility. A big step forward was made by Hurlburt, Toomre & Massaguer (1986) and Hurlburt et al. (1994), with fully non-linear, compressible, 2D, Cartesian simulations of overshooting/penetrative convection. Note that these two papers also introduce yet another way of creating a radiative/convective system, by using a vertically varying thermal conductivity profile. This creates a variation in the background radiative temperature gradient in the different layers that can be selected to achieve different stability properties, and the background model ultimately takes the form of stacked polytropes. This set-up naturally introduces the concept of 'stiffness' S as the ratio of the subadiabaticity of the stable region to the superadiabaticity of the unstable region. Most notably, these papers investigate the dependence of the depth δ of extended motions on the stiffness S, revealing two separate regimes: one associated with penetration ($\delta \propto S^{-1}$) and one with overshoot ($\delta \propto S^{-1/4}$) (more on this topic later). These studies also demonstrate the generation of gravity waves in the stable interior by the overshooting, both in fully compressible simulations (e.g. Hurlburt et al. 1986, see also Pratt et al. 2017) and in anelastic ones (e.g. Rogers & Glatzmaier 2005; Brun, Miesch & Toomre 2011). Freytag, Ludwig & Steffen (1996) performed fully compressible 2D, radiation-hydrodynamics simulations of the narrow convection zones sandwiched between stable layers created by a complex equation of state including ionization found in A-type stars and cool DA white dwarfs. This paper notably finds deep overshooting, attributes the exponential drop off observed in the overshoot velocity to the stable 'tail' of the convectively unstable modes excited in the convection zone, and derives a depth-dependent diffusion coefficient to describe the corresponding mixing. This exponential formulation for mixing by overshooting convection is now commonly used in stellar evolution codes (e.g. Herwig 2000; Paxton et al. 2011, 2013; Sukhbold & Woosley 2014).

3D simulations of the Cartesian stacked polytropic model became possible in the latter part of the 1990s. Singh, Roxburgh & Chan (1995), Singh, Roxburgh & Chan (1998), and Saikia et al. (2000), for instance, present a series of low-resolution large-eddy simulations with subgrid scale modelling while Muthsam et al. (1995) present low-resolution finite-difference models. All of these are fully compressible, and mostly appear to confirm the ideas of the 2D simulations and analysis, including the various aforementioned scalings with the stiffness, S. Somewhat later, however, Brummell, Clune & Toomre (2002) presented a more comprehensive parameter survey performed with high-resolution, direct numerical simulations (DNS), including much more turbulent cases and a wider range of S. That work finds only overshooting and no true penetration, even in the parameter regimes where it would be most likely to occur, such as high Rayleigh number, low Prandtl number, and low S. Instead, the transition from adiabatic to subadiabatic stratifications is seen to be rather smooth, and takes place across an extended partially mixed region. The authors attribute this mainly to the low filling factor of the downflowing convective plumes in the turbulent compressible case, arguing that the earlier low-resolution 3D models only found penetration because they were far more laminar and almost 2D.

In parallel with the predominantly numerical efforts described above, a variety of more phenomenological models have been proposed to date. Early works in stellar evolution typically use a non-local formulation of mixing-length theory (e.g. Spiegel 1963; Shaviv & Salpeter 1973; Cogan 1975; Maeder 1975), with results that vary widely depending on specific assumptions

associated with the non-local integration scale, as criticized by Renzini (1987). As the aforementioned numerical simulations began to provide more insight into the dynamics of overshooting convection, phenomenological models have shifted towards more realistic representations of the convective flows. In addition to the semi-analytical weakly non-linear theories discussed earlier, van Ballegooijen (1982), for instance, includes the effect of the horizontal flows near the base of the convection zone via linear convective roll modes with an assumed non-linear saturation amplitude, with similar results to those of the mixing length theory (that only includes vertical motions). Schmitt, Rosner & Bohn (1984) builds on the emerging idea that the convective motions are more plume-dominated than cellular by using a meteorological model for plumes in a stable stratification with entrainment (Morton, Taylor & Turner 1956); the model formally reduces to the mixing length model of Shaviv & Salpeter (1973) in the limit of zero entrainment. Schmitt et al. (1984) find that shallow penetration is likely in the solar case, with the depth being dependent mainly on the velocity and filling factor of the plumes at the base of the convection zone (and insensitive to other parameters, such as the entrainment rate), and that the transition to radiative dynamics below likely takes place through a very thin thermal adjustment boundary layer.

The work of Zahn (1991) simplifies these ideas by applying scaling arguments to the problem. He separates the dynamics below the convection zone into a true penetrative region (where the motions are vigourous enough to mix the background stratification to adiabatic) and a thermal boundary layer containing overshooting. His model recovers the dependence of the penetration depth on the typical convection zone velocity ($\propto w^{3/2}$) and on the assumed filling factor of the plumes ($\propto f^{1/2}$) found numerically by Schmitt et al. (1984), which is interesting since both models make rather different assumptions on the nature of the plumes. Zahn (1991) also finds that the depth of this layer depends on the gradient of the conductivity profile, leading to a value of about 50 per cent of a pressure scale height in the solar case. Finally, Zahn's thermal boundary layer is very thin as in Schmitt et al. (1984). A similar model is used in Hurlburt et al. (1994) but with the smooth conductivity profile replaced by a more abrupt piecewise-constant one corresponding to their stacked polytrope numerical simulations. Writing their predictions for the depth δ of the mixed layers in terms of the stratification (stiffness) ratio, S, they can explain their aforementioned observed scaling laws, namely $\delta \propto S^{-1}$ for true penetration and $\delta \propto S^{-1/4}$ for the thermal boundary (overshoot) layer. They explain the transition in the scalings with increasing S as a tradeoff between the increase in buoyancy braking and the decrease in local Péclet number.

Rempel (2004) builds upon these previous works with a semi-analytical model that follows a distribution of plumes throughout both the convection zone and overshoot region and includes their interaction with the upflows. This model thereby essentially incorporates non-locality and entrainment and further allows departures from the parameter regimes where mixing length theory is most likely to work (i.e. towards parameter regimes accessible by numerical simulations). Its predictions mirror the findings of Schmitt et al. (1984) and Zahn (1991) but also reveal the extra dependencies of the overshoot characteristics on the total energy flux (determining the vigour of the eddies in the convection zone) and the assumed degree of mixing by entrainment. In particular, the dependence on the non-local convective efficiency is postulated to explain the presence of true penetration in mixing length results (which are necessarily highly turbulent) by contrast with its absence in the 3D simulations (where the degree of turbulence is limited due to numerical issues). Furthermore, this approach demonstrates that an ensemble of plumes with a distribution of velocities behaves quite differently from one where all the plumes have the same assumed velocity. In particular, the former results in a much smoother thermal transition between the penetration layer and the deeper radiative stratification than the latter, which has important observational implications for helioseismology (e.g. Monteiro, Christensen-Dalsgaard & Thompson 1994; Monteiro & Thompson 1998).

To summarize, the main robust conclusions of these numerical and phenomenological modelling efforts are that penetration and overshooting can take place down to some fraction of the pressure scale height that depends on the exit velocity and the filling factor (or scale) of the downflowing motions at the base of the convection zone. The velocity of downflowing plumes depends on the strength of the convection itself in a non-local, bulk sense, requiring high Péclet number for any chance of penetration. Meanwhile the filling factor of these plumes depends on many factors such as geometry (2D versus 3D), compressibility, stratification, and on a turbulent entrainment efficiency that remains poorly constrained. These models also reveal dynamical differences between smooth and abrupt transitions in the background stratification associated with both radiative and adiabatic temperature gradients (e.g. Zahn 1991; Rogers & Glatzmaier 2005).

Moving forward, the next natural step towards a better understanding of overshooting and penetration should involve 3D simulations in a spherical geometry and some effects of compressibility – either using fully compressible equations or anelastic equations. Although quite a number of simulations of this variety have actually been performed, the vast majority of them have not explicitly examined the penetrative/overshooting question, since they were directed at the global dynamo problem or the solar tachocline problem (for recent efforts, see e.g. Brun, Browning & Toomre 2005; Browning et al. 2006, 2007; Miesch, Brun & Toomre 2006; Ghizaru, Charbonneau & Smolarkiewicz 2010; Brun et al. 2011; Racine et al. 2011; Strugarek, Brun & Zahn 2011). Since such dynamo-directed models require significant turbulence, the considerable expense of these computational efforts has been dedicated to a small number of simulations that are the most relevant, rather than an exhaustive study of parameter space. Notable exceptions are the work of Browning, Brun & Toomre (2004) and Brun et al. (2017) who look at differential rotation and overshoot in core-convective stars and solar-type stars, respectively. In both cases, however, the set of simulations presented are far from actual stellar parameters in terms of actual diffusivities and vary quantities such as the rotation rate and/or the stellar mass, rather than input parameters that more directly control the strength of the convection and the stratification of the nearby radiative zone. Because of this, the results cannot easily be used to form a prognostic model for overshoot and penetration in more stellar-like conditions.

This paper therefore presents a parametric survey of stellar-like overshooting convection in a 3D spherical geometry using DNS. As a first step towards understanding the full problem, we consider Boussinesq dynamics (Spiegel & Veronis 1960) only, arguing that in many instances the interface between radiative and convective regions is located very deep in the interior of the star where this approximation is not perfect but reasonable. For example, the pressure scale height at the bottom of the solar CZ is approximately 1/3 of the depth of the solar CZ. This means that convective motions on scales substantially smaller than this are well approximated by the Boussinesq approximation, but that larger scale motions would be subject to compressibility effects that are ignored here. We also ignore rotation in order to isolate the effects of geometry (asymme-

try) and of the model parameters. Our goal is to quantitatively characterize various aspects of the dynamics of the overshoot/penetration zone, in particular, the relationship between the typical velocity of convective eddies and the amount of mixing induced beyond the edge of the original convection zone. Ultimately, we shall answer the question of when one should expect overshoot or true penetration in a star and provide a usable prescription for mixing by overshooting convection that can easily be incorporated into 1D stellar structure models.

The paper is organized as follows. In Section 2, we describe the model configuration along with the initial conditions and the boundary conditions. In Section 3, we present some general characteristics of a canonical simulation and we describe three characteristic length-scales. In Section 4, we provide a model for the kinetic energy profile below the base of the convection zone. In Section 5, we focus on thermal mixing in the radiative zone due to the overshooting of the turbulent motions in the stable region. Finally, in Section 6, we summarize our results, provide comparisons with previous numerical work, and discuss the implications of these results in the solar and stellar overshooting dynamics.

2 MODEL SET-UP

We are interested in studying a two-layered system consisting of a convectively unstable zone (CZ) overlying a radiative zone (RZ) which is everywhere locally stable to convection according to the Schwarzschild criterion. The numerical model used builds upon the purely convective spherical shell set-up described in Korre, Brummell & Garaud (2017) extended to include a convectively stable inner spherical shell beneath the unstable one. Our chosen shell has an outer radius r_o, and inner radius $r_i = 0.2r_o$, with the CZ–RZ interface located at $r_t = 0.7r_o$. This geometry was chosen to mimic that of the Sun, as an example of a fairly typical low-mass star. The position of the inner boundary does not affect any of our results, as long as $r_i \ll r_t$. The selection of the convection zone aspect ratio r_t/r_o is expected to affect the results, on the other hand. However, we have chosen to keep it fixed since there are already many other parameters that need to be varied in the simulations (see below).

In an attempt to be relevant for stellar contexts, we adopt a number of specific dynamical ingredients. We solve the 3D Navier–Stokes equations under the Spiegel & Veronis (1960) Boussinesq approximation, which takes into account a non-zero adiabatic temperature gradient to account for weak compressibility. We assume constant thermal expansion coefficient α, viscosity ν, thermal diffusivity κ, adiabatic temperature gradient $\mathrm{d}T_{\mathrm{ad}}/\mathrm{d}r$, and gravity g. Note that these quantities would of course not be constant over the range $r = [0.2r_o, r_o]$ in a star – this assumption is made for simplicity. We fix the heat flux at the inner boundary to account for the energy generated from nuclear burning in the stellar core, whereas at the outer boundary we fix the temperature. While the latter does not realistically capture the more complex radiative transfer processes that are known to control the photospheric boundary conditions in solar-type stars, we use this approximation because it is simple, with the expectation that it does not affect the convective dynamics near the bottom of the convection zone. Finally, we perform all of our simulations in a low Prandtl number regime (where the Prandtl number is the ratio of the viscosity to thermal diffusivity), which is again more relevant in the astrophysical context. To the authors' knowledge, this is the first time that penetrative convection is being studied in a Boussinesq spherical shell geometry with the temperature boundary conditions as described above and in the low Prandtl number regime.

We let $T(r, \theta, \phi, t) = T_{\mathrm{rad}}(r) + \Theta(r, \theta, \phi, t)$ where T_{rad} is the temperature profile our system would have under pure radiative equilibrium, and where Θ describes temperature fluctuations away from that radiative equilibrium. As part of the Boussinesq approximation, a linear relationship is assumed between the temperature and density perturbations such that $\rho/\rho_m = -\alpha\Theta$, where ρ_m is the mean density of the background fluid. Then, the governing Boussinesq equations are (Spiegel & Veronis 1960)

$$\nabla \cdot \boldsymbol{u} = 0, \tag{1}$$

$$\frac{\partial \boldsymbol{u}}{\partial t} + \boldsymbol{u} \cdot \nabla \boldsymbol{u} = -\frac{1}{\rho_m}\nabla p + \alpha\Theta g \boldsymbol{e_r} + \nu\nabla^2 \boldsymbol{u}, \tag{2}$$

and

$$\frac{\partial \Theta}{\partial t} + \boldsymbol{u} \cdot \nabla\Theta + u_r\left(\frac{\mathrm{d}T_{\mathrm{rad}}}{\mathrm{d}r} - \frac{\mathrm{d}T_{\mathrm{ad}}}{\mathrm{d}r}\right) = \kappa\nabla^2\Theta, \tag{3}$$

where $\boldsymbol{u} = (u_r, u_\theta, u_\phi)$ is the velocity field and p is the pressure perturbation away from hydrostatic equilibrium.

One way to set up the desired two-layered system is by ensuring that $\mathrm{d}T_{\mathrm{rad}}/\mathrm{d}r - \mathrm{d}T_{\mathrm{ad}}/\mathrm{d}r$ is negative in the CZ and positive in the RZ. Since T_{rad} is the temperature profile at radiative equilibrium, and since we considered that ν and κ are constant, the only way to ensure that its gradient changes significantly (aside from geometric effects) is to assume the existence of a heating source localized near r_t, such that

$$\kappa\nabla^2 T_{\mathrm{rad}} = -H_s(r). \tag{4}$$

The function $T_{\mathrm{rad}}(r)$ is the solution of this equation with the boundary conditions

$$-\kappa\left.\frac{\mathrm{d}T_{\mathrm{rad}}}{\mathrm{d}r}\right|_{r=r_i} = F_{\mathrm{rad}}, \tag{5}$$

where F_{rad} is the temperature flux per unit area through the inner boundary and

$$T(r_o) = T_o. \tag{6}$$

Integrating equation (4) once yields

$$\kappa\frac{\mathrm{d}T_{\mathrm{rad}}}{\mathrm{d}r} + \left(\frac{r_i}{r}\right)^2 F_{\mathrm{rad}} = -\frac{1}{r^2}\int_{r_i}^{r} H_s(r')r'^2\,\mathrm{d}r', \tag{7}$$

showing that we can generate any functional form we desire for $\mathrm{d}T_{\mathrm{rad}}/\mathrm{d}r$ with a suitable choice of $H_s(r)$. Note that in practice (see below), the exact expressions for $H_s(r)$ and $T_{\mathrm{rad}}(r)$ are not needed.

We non-dimensionalize the problem by using $[l] = r_o$, $[t] = r_o^2/\nu$, $[u] = \nu/r_o$, and $[T] = |\mathrm{d}T_o/\mathrm{d}r - \mathrm{d}T_{\mathrm{ad}}/\mathrm{d}r|r_o$ as the unit length, time, velocity, and temperature, respectively, where $\mathrm{d}T_o/\mathrm{d}r \equiv \mathrm{d}T_{\mathrm{rad}}/\mathrm{d}r|_{r=r_o}$ is the radiative temperature gradient at the outer boundary. Then, we can write the non-dimensional equations as

$$\nabla \cdot \boldsymbol{u} = 0, \tag{8}$$

$$\frac{\partial \boldsymbol{u}}{\partial t} + \boldsymbol{u} \cdot \nabla \boldsymbol{u} = -\nabla p + \frac{\mathrm{Ra_o}}{\mathrm{Pr}}\Theta \boldsymbol{e_r} + \nabla^2 \boldsymbol{u}, \tag{9}$$

and

$$\frac{\partial \Theta}{\partial t} + \boldsymbol{u} \cdot \nabla\Theta + \beta(r)u_r = \frac{1}{\mathrm{Pr}}\nabla^2\Theta. \tag{10}$$

In all that follows, all the variables and parameters are now implicitly non-dimensional. This introduces the Prandtl number, Pr, and the

global Rayleigh, $\mathrm{Ra_o}$, defined as

$$\mathrm{Pr} = \frac{\nu}{\kappa} \quad \text{and} \quad \mathrm{Ra_o} = \frac{\alpha g \left| \frac{\mathrm{d}T_\mathrm{o}}{\mathrm{d}r} - \frac{\mathrm{d}T_\mathrm{ad}}{\mathrm{d}r} \right| r_\mathrm{o}^4}{\kappa \nu}, \tag{11}$$

as well as the function $\beta(r)$ which is given by

$$\beta(r) = \frac{\frac{\mathrm{d}T_\mathrm{rad}}{\mathrm{d}r} - \frac{\mathrm{d}T_\mathrm{ad}}{\mathrm{d}r}}{\left| \frac{\mathrm{d}T_\mathrm{o}}{\mathrm{d}r} - \frac{\mathrm{d}T_\mathrm{ad}}{\mathrm{d}r} \right|}. \tag{12}$$

By suitably selecting $H_s(r)$, and therefore $T_\mathrm{rad}(r)$, we can create a profile for $\beta(r)$ that results in a convectively stable region for $r_\mathrm{i} \leq r < r_\mathrm{t}$ and an unstable region for $r_\mathrm{t} \leq r \leq r_\mathrm{o}$. Here, we choose to impose a function $\beta(r)$ of the form

$$\beta(r) = \begin{cases} -S \tanh\left(\dfrac{r - r_\mathrm{t}}{d_\mathrm{in}}\right) & \text{when } r < r_\mathrm{t}, \\ -\tanh\left(\dfrac{r - r_\mathrm{t}}{d_\mathrm{out}}\right) & \text{when } r \geq r_\mathrm{t}, \end{cases} \tag{13}$$

where d_in and d_out constrain the width of the imposed radiative–convective boundary, while S is the stiffness parameter that measures the relative stability of the radiative and the convective zones. Note that d_in is chosen such that the derivative of $\beta(r)$ is continuous at $r_\mathrm{t} = 0.7$, which implies that $d_\mathrm{in} = S d_\mathrm{out}$. The quantity d_out^{-1} is the derivative of the function β at $r = r_\mathrm{t}$, and therefore describes the steepness of its profile. In this model $\beta(r)$ tends to -1 in the bulk of the convection zone, and to S in the bulk of the radiative zone. In stars, this is of course not the case, and $\beta(r)$ can vary very significantly within both convective and radiative zones, so this model is chosen for simplicity but with the ability to explore certain questions raised in the introduction related to the effect of the stiffness and the abruptness of the transition. Note that in the Sun, $|\beta(r)|$ decreases substantially from the top to the base of the convection zone (see Korre et al. 2017), the slope of the transition into the radiation zone is rather smooth, and $|\beta(r)|$ in the radiative zone is of the same order as $|\beta|$ in the bulk of the convection zone (which implies that S would be of the order of unity).

The function β can also be expressed as minus the ratio of the local Rayleigh number $\mathrm{Ra}(r)$ to $\mathrm{Ra_o}$, namely

$$\beta(r) = -\frac{\mathrm{Ra(r)}}{\mathrm{Ra_o}}, \tag{14}$$

where

$$\mathrm{Ra}(r) = -\frac{\alpha g \left(\frac{\mathrm{d}T_\mathrm{rad}}{\mathrm{d}r} - \frac{\mathrm{d}T_\mathrm{ad}}{\mathrm{d}r} \right) r_\mathrm{o}^4}{\kappa \nu}, \tag{15}$$

and where the minus sign in equation (15) ensures that $\mathrm{Ra}(r)$ is positive in convective regions. In Fig. 1, we show representative profiles of $\beta(r)$ in order to demonstrate their dependence on the two parameters S and d_out. Higher values of S result in a larger jump in $\beta(r)$ from the base of the CZ inward, while lower values of d_out at fixed S lead to a steeper and more sudden transition.

In order to study the dynamics of our two-layered system and understand the mixing processes that occur due to the propagation of the convective motions into the stable layer, we have run 3D DNS solving the Boussinesq equations in a spherical shell, exactly as outlined above, using the PARODY code (Dormy, Cardin & Jault 1998; Aubert, Aurnou & Wicht 2008). In all of our simulations, the Prandtl number is fixed and equal to Pr=0.1. The boundary conditions for the temperature are such that we have fixed flux at the inner boundary that translates into a no-flux boundary condition

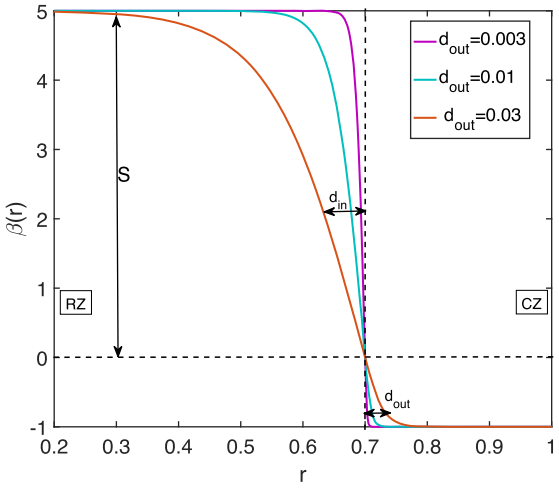

Figure 1. The profile of $\beta(r)$ versus the radius r, for $S = 5$ and three different d_out values.

for the perturbations Θ, $\partial\Theta/\partial r|_{r_\mathrm{i}} = 0$, and fixed temperature at the outer boundary that translates into a zero temperature boundary condition for Θ, $\Theta(r_\mathrm{o}) = 0$. For the velocity, we employ stress-free boundary conditions. Each simulation is evolved from a zero initial velocity and small-amplitude perturbations in the temperature field until a statistically stationary and thermally relaxed state is achieved. To determine when this is the case, we look both at the total kinetic energy per unit volume in the domain, $E(t) = \frac{1}{2}(u_r^2 + u_\theta^2 + u_\phi^2)$, and at the temperature perturbation gradient at the surface.

We have run a large number of simulations, whose input parameters are summarized in Table 1. In Section 3, we present an in-depth study of a typical simulation, focusing on identifying measures of the dynamics of overshooting and/or penetrative convection in the vicinity of the CZ–RZ interface. In Sections 4 and 5 we then look in turn at selected properties of our results across all available simulations.

3 GENERAL CHARACTERISTICS OF A TYPICAL SIMULATION

Throughout the paper, we define the time and spherical average of a quantity as

$$\bar{q}(r) = \frac{1}{4\pi(t_2 - t_1)} \int_{t_1}^{t_2} \int_0^{2\pi} \int_0^{\pi} q(r, \theta, \phi, t) \sin\theta \, \mathrm{d}\theta \, \mathrm{d}\phi \, \mathrm{d}t, \tag{16}$$

where t_1 and t_2 are an initial and a final time, taken once the system has reached a statistically stationary state. We sometimes choose to present properties of the downflows and upflows separately. Therefore, we also define the average over downflows and upflows only as

$$\bar{q}_\mathrm{down}(r) = \frac{1}{A_\mathrm{down}(t_2 - t_1)} \int_{t_1}^{t_2} \int_0^{2\pi} \int_0^{\pi} q(r, \theta, \phi, t) H(-u_r) \sin\theta \, \mathrm{d}\theta \, \mathrm{d}\phi \, \mathrm{d}t, \tag{17}$$

$$\bar{q}_\mathrm{up}(r) = \frac{1}{A_\mathrm{up}(t_2 - t_1)} \int_{t_1}^{t_2} \int_0^{2\pi} \int_0^{\pi} q(r, \theta, \phi, t) H(u_r) \sin\theta \, \mathrm{d}\theta \, \mathrm{d}\phi \, \mathrm{d}t, \tag{18}$$

Table 1. Columns 1–7: summary of all input parameters and resolution of our simulations. Column 8 reports on the length-scale δ_G discussed in Section 3. Column 9 reports on the length-scale δ_{en} discussed in Section 4. Column 10 reports on the length-scale δ_Θ discussed in Section 3, and column 11 reports on δ_u discussed in Section 3. Columns 12 and 13 report on Pe and Pe_{ov} as discussed in Section 3. The respective Reynolds numbers are Re=10Pe and $Re_{ov} = 10Pe_{ov}$.

Case #	S	d_{out}	d_{in}	Ra_o	Pr	$N_r \times N_\theta \times N_\phi$	δ_G	δ_{en}	δ_Θ	δ_u	Pe	Pe_{ov}
1	100	0.0003	0.03	10^6	0.1	$350 \times 192 \times 192$	0.020	0.017	0.059	0.048	7.3	0.5
2	5	0.003	0.015	10^6	0.1	$300 \times 192 \times 192$	0.060	0.045	0.150	0.130	8.4	1.7
3	10	0.003	0.03	10^6	0.1	$300 \times 192 \times 192$	0.049	0.039	0.130	0.100	8.2	1.3
4	20	0.003	0.06	10^6	0.1	$300 \times 192 \times 192$	0.044	0.037	0.110	0.092	8.2	1.2
5	2	0.01	0.02	10^6	0.1	$300 \times 192 \times 192$	0.096	0.069	0.240	0.220	8.9	2.9
6	5	0.01	0.05	10^6	0.1	$300 \times 192 \times 192$	0.071	0.057	0.170	0.150	8.8	2.1
7	10	0.01	0.1	10^6	0.1	$300 \times 192 \times 192$	0.064	0.054	0.150	0.130	8.6	1.8
8	5	0.03	0.15	10^6	0.1	$300 \times 192 \times 192$	0.091	0.078	0.220	0.190	9.0	2.7
9	10	0.03	0.3	10^6	0.1	$300 \times 192 \times 192$	0.089	0.077	0.210	0.190	9.0	2.6
10	5	0.05	0.25	10^6	0.1	$300 \times 192 \times 192$	0.104	0.091	0.260	0.230	9.0	3.1
11	5	0.003	0.015	10^7	0.1	$400 \times 288 \times 320$	0.047	0.034	0.110	0.094	21.7	3.4
12	10	0.003	0.03	10^7	0.1	$400 \times 288 \times 320$	0.038	0.030	0.090	0.075	21.7	2.7
13	20	0.003	0.06	10^7	0.1	$400 \times 288 \times 320$	0.035	0.029	0.085	0.070	21.5	2.5
14	5	0.01	0.05	10^7	0.1	$400 \times 288 \times 320$	0.057	0.045	0.140	0.120	22.3	4.2
15	10	0.01	0.1	10^7	0.1	$400 \times 288 \times 320$	0.052	0.043	0.120	0.104	22.0	3.8
16	5	0.03	0.15	10^7	0.1	$400 \times 288 \times 320$	0.077	0.062	0.170	0.150	22.6	5.8
17	10	0.03	0.3	10^7	0.1	$400 \times 288 \times 320$	0.075	0.062	0.170	0.150	22.5	5.6
18	5	0.05	0.25	10^7	0.1	$400 \times 288 \times 320$	0.090	0.073	0.200	0.180	22.1	6.6
19	5	0.003	0.015	10^8	0.1	$585 \times 516 \times 640$	0.035	0.026	0.080	0.069	50.5	5.9
20	10	0.003	0.03	10^8	0.1	$585 \times 516 \times 640$	0.030	0.024	0.068	0.058	49.7	4.9
21	20	0.003	0.06	10^8	0.1	$585 \times 516 \times 640$	0.028	0.024	0.063	0.054	49.6	4.6
22	5	0.01	0.05	10^8	0.1	$585 \times 516 \times 640$	0.045	0.036	0.097	0.089	51.6	7.8
23	10	0.01	0.1	10^8	0.1	$585 \times 516 \times 640$	0.043	0.035	0.094	0.085	51.5	7.3
24	5	0.03	0.15	10^8	0.1	$585 \times 516 \times 640$	0.063	0.050	0.140	0.120	51.5	10.9
25	10	0.03	0.3	10^8	0.1	$585 \times 516 \times 640$	0.062	0.050	0.130	0.120	51.3	10.6

where H is the Heaviside function, A_{down} is the area covered by the downflows, namely

$$A_{down}(r) = \frac{1}{t_2 - t_1} \int_{t_1}^{t_2} \int_0^{2\pi} \int_0^{\pi} H(-u_r) \sin\theta \, d\theta \, d\phi \, dt, \quad (19)$$

and A_{up} is the area of the upflows such that

$$A_{up}(r) = \frac{1}{t_2 - t_1} \int_{t_1}^{t_2} \int_0^{2\pi} \int_0^{\pi} H(u_r) \sin\theta \, d\theta \, d\phi \, dt. \quad (20)$$

We begin by presenting the results of a typical run where $S = 5$, $d_{out} = 0.003$, and $Ra_o = 10^7$ (Case 11 in Table 1), which illustrates some of the most basic characteristics observed in almost all of our simulations. Table 1 summarizes its input parameters, resolution, and some of the quantities of interest discussed below. The profile of $\beta(r)$ corresponding to these parameters is shown as the purple line in Fig. 1.

Fig. 2(a) shows the evolution of the total kinetic energy per unit volume E as a function of time t in the simulation. We observe the initial development of the convective instability in the interval $t \in [0, 0.01]$ as a large spike, followed by its non-linear saturation. The system reaches a statistically steady state in this global quantity very fast because the energy is dominated by the dynamics of the CZ that rapidly equilibrates. However, we must also make sure that the system reaches global thermal equilibrium. This occurs on a much slower time-scale, which depends on the radiative diffusion through the RZ. In our simulations, we estimate that this has occurred when $\partial\Theta/\partial r|_{r=r_o}$ is statistically stationary and close to zero. This happens around $t = 0.04$ in this case. This is almost 200 times slower than the respective thermal relaxation time of the overshoot layer. The latter is faster since it is easier for the overshoot layer to thermally adjust compared with the whole radiative shell.

In Fig. 3, we present snapshots of meridional slices of the velocity components as a function of depth and latitude, for a selected longitude, all taken at the same time t during the statistically stationary state. They clearly show that the convective motions driven within the CZ are not confined to that region, but instead, travel some distance beyond the CZ–RZ interface (marked by the inner black line at $r_t = 0.7$). As we shall demonstrate, there are many ways in which one can quantitatively study the effect of convective motions that overshoot below the base of the CZ, such as through their kinetic energy, through their effect on the mean temperature profile, as well as through their vertical coherence. Each of these diagnostics presents a different facet of the problem that we will try to reconcile through modelling in the following sections.

We begin with Fig. 2(b) that shows the non-dimensional kinetic energy profile $\bar{E}(r)$ given by

$$\bar{E}(r) = \frac{1}{2}\overline{(u_r^2 + u_\theta^2 + u_\phi^2)}, \quad (21)$$

as black triangles. On the same figure, we plot the radial component of the kinetic energy (dashed green line), the vertical kinetic energy of the downflows (dotted cyan line), as well as the horizontal component of the kinetic energy (red line) given, respectively, by

$$\bar{E}_r(r) = \frac{1}{2}\overline{u_r^2}, \quad \bar{E}_{r,down}(r) = \frac{1}{2}\overline{u_{r,down}^2}, \quad \text{and}$$
$$\bar{E}_h(r) = \frac{1}{2}\overline{(u_\theta^2 + u_\phi^2)}. \quad (22)$$

There is clearly significant kinetic energy below the CZ corresponding to overshooting. Below the CZ, the motions are no longer convectively driven and must decelerate. This causes $\bar{E}(r)$ to decrease sharply inward from the base of the convection zone. Furthermore, we see that the contributions to $\bar{E}(r)$ coming from

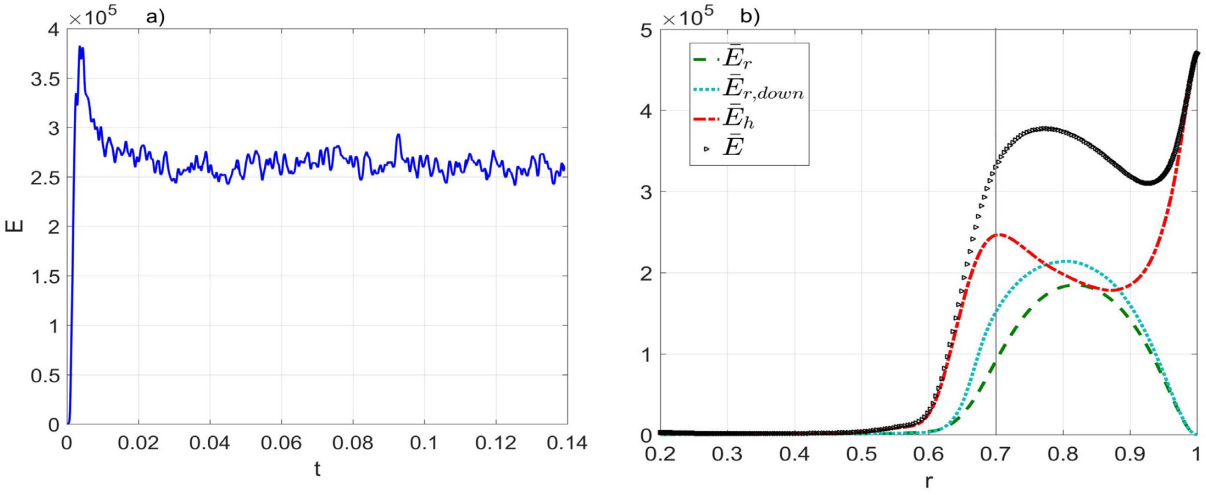

Figure 2. (a) Non-dimensional kinetic energy per unit volume as a function of time for a typical simulation with $S = 5$, $d_{\rm out} = 0.003$, and $\mathrm{Ra_o} = 10^7$. (b) Time-averaged non-dimensional kinetic energy profiles as a function of radius, for the same simulation, where $\bar{E}_r$ is the total kinetic energy (black triangles), $\bar{E}_r$ is the radial component of the kinetic energy (dashed green line), $\bar{E}_{r,\rm down}$ is the vertical kinetic energy of the downflows (dotted cyan line), and $\bar{E}_{\rm h}$ is the horizontal component of the kinetic energy (red line).

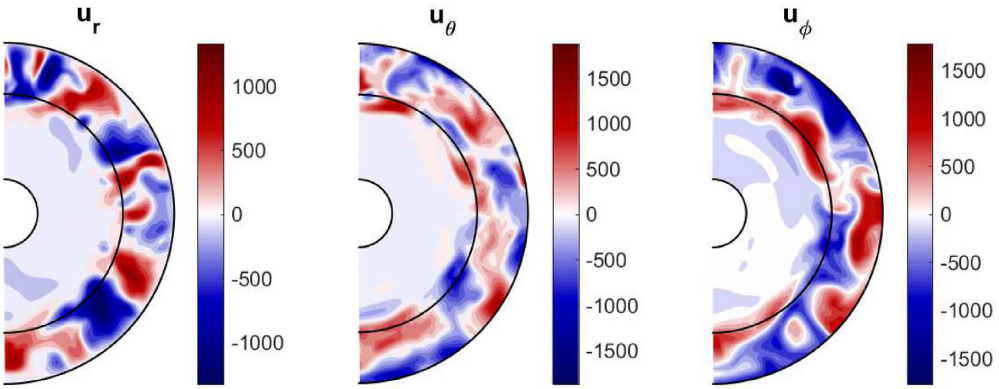

Figure 3. Snapshot slice showing the velocities u_r, u_θ, and u_ϕ on a selected meridional plane for a typical simulation of $S = 5$, $d_{\rm out} = 0.003$, and $\mathrm{Ra_o} = 10^7$. The inner black line represents the base of the convection zone at $r_{\rm t}$.

radial and horizontal motions behave very differently from one another. The vertical kinetic energy $\bar{E}_r$ peaks in the middle of the CZ, and then decreases inward, a result we attribute to a deceleration of the downflows as they approach the CZ–RZ interface at $r_{\rm t} = 0.7$ from above. This can indeed be verified in the profile of $\bar{E}_{r,\rm down}$ that has the same properties, although we also see that it is a little larger, indicating that downflows must be on average stronger (but narrower) than the upflows (this can be verified by a direct inspection of $A_{\rm up}$ and $A_{\rm down}$, not shown). Meanwhile, the horizontal kinetic energy increases substantially near the bottom of the convection zone. Thus, there is an exchange of kinetic energy between the vertical and the horizontal flows, which we interpret as the result of a deflection of the vertical plumes towards the horizontal. While this may seem somewhat expected, it is interesting to see that this occurs in the bulk of the CZ and not only near or below the CZ–RZ interface, implying that the presence of this interface is felt in a highly non-local way throughout the entire convection zone. This result is not an artefact of the Boussinesq approximation, since it is also seen in anelastic and fully compressible 2D simulations (e.g. Rogers & Glatzmaier 2005; Pratt et al. 2017) and in 3D fully compressible simulations (e.g. Singh et al. 1995; Brummell et al. 2002).

From the CZ–RZ interface downwards, we observe a rapid decrease in $\bar{E}(r)$, which is expected from the stabilizing effect of the stratification. Note that since the energy in the vertical motions has already decreased significantly even before reaching the CZ–RZ interface, most of the remaining energy below the base of the CZ comes from horizontal motions only. This leads to the conclusion that horizontal motions are dominant in the average sense below the CZ and therefore have to be considered in the study of convective overshooting dynamics, as in the models of e.g. van Ballegooijen (1982) and Rempel (2004).

In Fig. 4, we plot the total kinetic energy $\bar{E}(r)$ on a log scale to clarify its features below $r_{\rm t}$. We see that $\bar{E}(r)$ drops significantly faster than exponentially with depth below the CZ in contrast with the model proposed by Freytag et al. (1996; also see Herwig 2000). In fact, we find that a Gaussian function of the kind

$$f(r) = A \exp\left(-\frac{(r - r_{\rm t})^2}{2\delta_{\rm G}^2}\right) \tag{23}$$

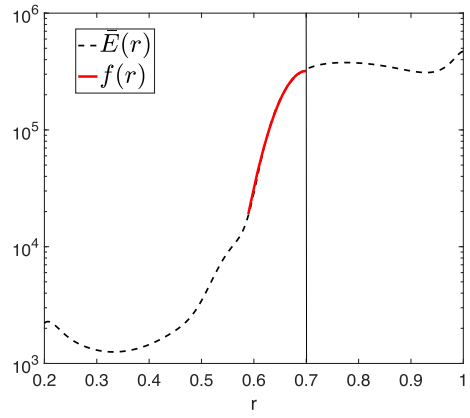

Figure 4. Kinetic energy profile $\bar{E}(r)$ for $S = 5$, $d_{\rm out} = 0.003$, and $\mathrm{Ra_o} = 10^7$ against the radius r. The red solid line is the fitted curve of the kinetic energy profile on this interval.

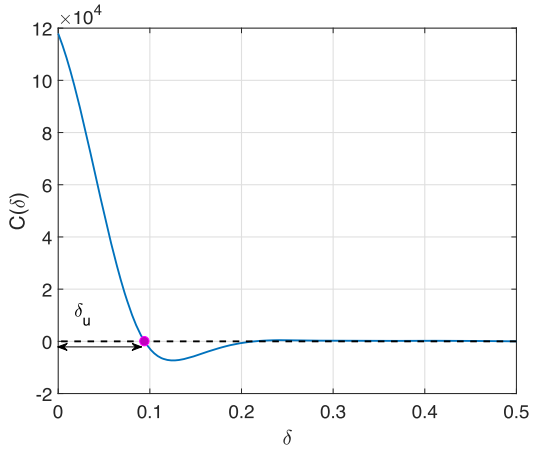

Figure 5. Profile of $C(\delta)$ against δ for $S = 5$, $d_{\rm out} = 0.003$, and for $\mathrm{Ra_o} = 10^7$.

with $\delta_{\rm G} = 0.047$ would be a much better fit to the profile of $\bar{E}(r)$, at least down to $r = 0.58$, as shown by the red solid line in Fig. 4. Below that point, the decay of the kinetic energy is closer to being exponential in the interval [0.47,0.58]. Even deeper down, $\bar{E}(r)$ flattens out, presumably as a result of the presence of the inner boundary. The Gaussian function $f(r)$ can be used to characterize the spherically averaged kinetic energy profile of overshooting motions below the CZ and is parametrized by its amplitude A and by its width $\delta_{\rm G}$. Therefore, $\delta_{\rm G}$ can be used to characterize the region of influence of convective motions in the stable RZ, at least energetically speaking and in an average sense.

An alternative measure is the distance that the strongest of the downflow motions travel into the stable region; therefore, we introduce the radial correlation function of the vertical velocity field in the downflows

$$C(\delta) = \frac{1}{4\pi(t_2 - t_1)} \int_{t_1}^{t_2} \int_0^{2\pi} \int_0^{\pi} u_r(r_{\rm t}, \theta, \phi) H(-u_r(r_{\rm t}, \theta, \phi)) \times u_r(r_{\rm t} - \delta, \theta, \phi) \sin\theta \, {\rm d}\theta \, {\rm d}\phi \, {\rm d}t. \tag{24}$$

This definition clearly favours the strongest downflows. Fig. 5 shows $C(\delta)$ for our reference simulation. As expected, C decreases with depth δ below the base of the CZ. Interestingly, we see that instead

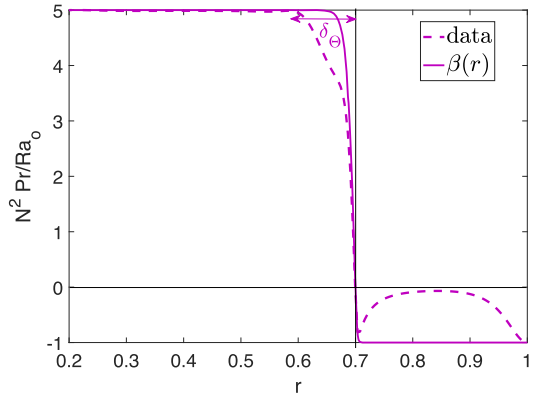

Figure 6. Non-dimensional square of the buoyancy frequency $\bar{N}^2\mathrm{Pr/Ra_o}$ (dashed line) compared with the background $N^2_{\rm rad}\mathrm{Pr/Ra_o}$ (solid line) for $S = 5$, $d_{\rm out} = 0.003$, and for $\mathrm{Ra_o} = 10^7$.

of merely approaching zero (which would indicate a gradual loss of correlation), $C(\delta)$ actually changes sign (here at $\delta = 0.094$). This implies that (1) the strongest downflows stop, on average, at a well-defined depth below the base of the CZ and that (2) there must be an upflow below each of these downflows. This can only occur if the downflow spreads laterally upon entering the RZ, and the lateral divergence of the fluid acts as a pump for the deeper upflow. This was in fact seen in all of our simulations. We therefore define a second measure of overshooting, the correlation depth $\delta_{\rm u}$ as the first zero of $C(\delta)$. This depth measures the average stopping distance of the strongest downflows. By comparison with Fig. 4, we see that $r_{\rm t} - \delta_{\rm u}$ corresponds to the radius where the kinetic energy switches from the Gaussian to the exponential profile below the CZ. This might be expected since a radical change in the dynamics of the fluid is taking place at $r_{\rm t} - \delta_{\rm u}$.

By focusing on the fluid motions until this point, we were only able to address the questions pertaining to overshooting rather than penetration. In order to see whether penetration occurs, we must see if substantial thermal (entropy) mixing is occurring. We therefore examine the non-dimensional spherically averaged buoyancy frequency $\bar{N}$ whose square is given by

$$\bar{N}^2(r) = \alpha g \left(\frac{{\rm d}\bar{T}}{{\rm d}r} - \frac{{\rm d}T_{\rm ad}}{{\rm d}r} \right) \frac{r_{\rm o}^4}{\nu^2} = \left(\beta(r) + \frac{{\rm d}\bar{\Theta}}{{\rm d}r} \right) \frac{\mathrm{Ra_o}}{\mathrm{Pr}}. \tag{25}$$

Fig. 6 shows the profile of $\bar{N}^2\mathrm{Pr/Ra_o}$ measured in our simulations along with the original imposed background profile $N^2_{\rm rad}(r)\mathrm{Pr/Ra_o} = \beta(r)$ as a solid line for reference. As expected, the convective motions in the bulk of the CZ (away from both the top boundary and the CZ–RZ interface) mix potential temperature and drive the mean radial temperature gradient towards an adiabatic state where $\bar{N}^2 \approx 0$. Below the CZ, we notice that the fluid motions do affect the thermal stratification, but not strongly enough to effectively extend the region where $\bar{N}^2 \approx 0$. This indicates that there is no penetration (in the strict definition of the term), but also shows that the resultant profile of $\bar{N}^2$ below $r_{\rm t}$ is much smoother than the originally imposed one. This partially mixed region, which defines an intermediate state that is neither pure penetrative convection nor pure overshooting, was found in nearly all of our simulations and this is investigated in detail in Section 5. This result is not entirely surprising. Indeed, the possibility of such an intermediate state was already discussed by Zahn (1991) and Schmitt et al. (1984) (albeit briefly), and 3D fully compressible simulations to date have reported similar findings (e.g. Brummell et al. 2002; Käpylä et al. 2017).

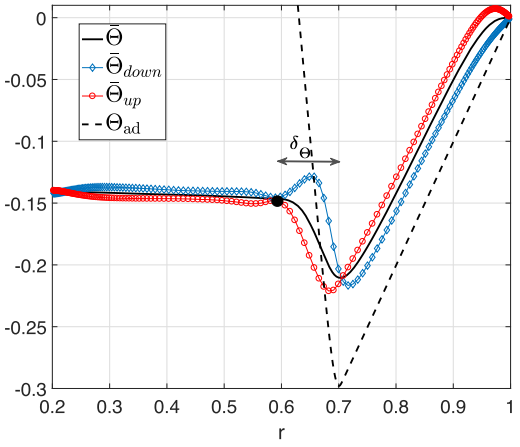

Figure 7. Temperature perturbations for $S = 5$, $d_{out} = 0.003$, and for $Ra_o = 10^7$ plotted along with the adiabatic temperature Θ_{ad}.

To better understand what might be the cause of this partial mixing, we now look at the details of the thermal transport. Fig. 7 shows the time- and spherically averaged temperature perturbations $\bar{\Theta}$ along with the mean temperature perturbation in the upflows ($\bar{\Theta}_{up}$) and downflows ($\bar{\Theta}_{down}$). We also show the temperature that a downflow travelling adiabatically from the surface (where $\Theta = 0$) would have as a function of r, namely $\Theta_{ad}(r) = -\int_{r_o}^{r} \beta(r')\,dr'$. We observe that the mean temperature gradient follows the adiabatic one quite closely in the CZ, but that $\bar{\Theta}$ is systematically larger than Θ_{ad} due to the existence of the outer thermal boundary layer. Moreover, we see that $\bar{\Theta}_{down}$ is lower than $\bar{\Theta}$ in the CZ, which is expected since cooler fluid parcels are accelerated downwards. Downflowing fluid parcels crossing the base of the CZ into the RZ begin to heat up through adiabatic compression and become significantly warmer than the mean. This provides them with an upward acceleration that gradually slows them down. Upflows follow a reverse pattern, where they are warmer than $\bar{\Theta}$ in the CZ, and cooler than $\bar{\Theta}$ in the RZ. Interestingly, we find that $\bar{\Theta}_{down}$ increases by a little just above the base of the CZ, a result that could either be due to non-linear mixing with the warmer upflows, or, to a diffusive heat flux coming from the much warmer perturbations below the base of the CZ.

We note that there is a point lower in the RZ (here, around $r = 0.6$), at which $\bar{\Theta}$, $\bar{\Theta}_{down}$, and $\bar{\Theta}_{up}$ approximately coincide. We therefore define a new length-scale δ_Θ that corresponds to the distance of this point from the CZ–RZ interface. Upflows and downflows are neutrally buoyant at $r = r_t - \delta_\Theta$. Below that level, we see that the correlation between the temperature and the direction of the flow becomes much weaker. This then implies that motion must no longer be of convective type and therefore this length-scale is another measure of where the dynamics change character. We find that $\delta_\Theta \simeq \delta_u$, and as mentioned before, $r_t - \delta_u$ also appears to coincide with the radius where the kinetic energy profile $\bar{E}(r)$ transitions from a Gaussian to an exponential (see Fig. 4). Finally, we also overlay the length-scale δ_Θ on Fig. 6 for comparison. Not surprisingly perhaps, we observe that δ_Θ coincides with the depth of the region in the RZ where $\bar{N}^2$ deviates most strongly from the radiative equilibrium profile. Therefore, δ_Θ provides a length-scale that is associated with the depth of (partial) thermal mixing in the stable region.

Another way of quantifying the transition from the fully mixed CZ, to the partially mixed overshoot layer, to the unmixed interior (below δ_Θ), is to look at the Péclet number, which is commonly defined as the ratio of advective to diffusive thermal time-scales. In the bulk of the convection zone, the Péclet number can be estimated as

$$\mathrm{Pe} = \frac{u_{cz}(r_o - r_t)}{\kappa} = 0.3 u_{rms}\mathrm{Pr}, \tag{26}$$

where the first expression contains only dimensional quantities and the second only contains non-dimensional ones. In the second expression, u_{rms} is the typical non-dimensional rms convective velocity (which can be extracted from the DNS). In the first expression, u_{cz} is its dimensional counterpart, with $u_{cz} = u_{rms}\nu/r_o$. In the overshoot layer on the other hand, an appropriate length-scale of eddies might be δ_G, and their non-dimensional rms velocity drops from u_{rms} to 0 over that length-scale, so we define the Péclet number as

$$\mathrm{Pe}_{ov} = u_{rms}\delta_G \mathrm{Pr}. \tag{27}$$

Note that the definition of any Péclet number is somewhat arbitrary, since there is ambiguity in the choices of the characteristic length and velocity scales. Using our particular choices above consistently, however, we can at least compare simulations. We find that Pe $\sim$22, and $\mathrm{Pe}_{ov} \sim 3$, for our canonical Case 11 of $S = 5$, $d_{out} = 0.003$, and $Ra_o = 10^7$. This finding is consistent with the expectation that the CZ is well mixed (with a large Pe), while the overshoot layer is only partially mixed (with Pe_{ov} of the order of unity). Note that associated Reynolds numbers can be calculated as Re=Pe/Pr = 10Pe (and similarly for Re_{ov}).

To summarize our results so far, our inspection of the dynamics observed in this simulation has suggested the definition of three distinct length-scales that each provides a different measure of the impact of convective motions on the underlying radiative zone. The first is the width δ_G of the Gaussian function fitted to the total kinetic energy profile below the base of the CZ. This parametrizes the profile of the decay of the turbulent kinetic energy with distance away from the CZ–RZ interface. The second is δ_u, given by the first zero of the radial correlation function of the downflows, $C(\delta)$. This can be interpreted as the length-scale down to which the strongest downflows travel before stopping. The third is the distance δ_Θ from the base of the CZ down to the point of neutral buoyancy where $\bar{\Theta} = \bar{\Theta}_{down} = \bar{\Theta}_{up}$ which is both a good estimate of the stopping of motions and of the vertical extent of the partially thermally mixed region in the stable RZ. We have found that $\delta_G < \delta_u \simeq \delta_\Theta$ for this simulation, a result that actually holds for all of our simulations (see Table 1). This suggests that while δ_G may provide an average view of the kinetic energy available for mixing below the base of the convection zone, much of that mixing is actually controlled by the strongest downflows, which overshoot much more deeply. These results are qualitatively consistent with the findings of Brummell et al. (2002) and Pratt et al. (2017) in fully compressible simulations, suggesting that the use of the Boussinesq approximation does not dramatically alter the dynamics of overshooting convection (at least near the base of a convective region deep within a star). In the following sections, we now look more broadly at how δ_G, δ_u, and δ_Θ vary with input parameters.

4 MODELLING THE KINETIC ENERGY PROFILE BELOW THE BASE OF THE CZ

In Section 3, we argued that the kinetic energy profile just below the base of the CZ resembles the Gaussian function $f(r)$ given in (23). Fig. 8 shows that this is the case in all of our simulations, which span

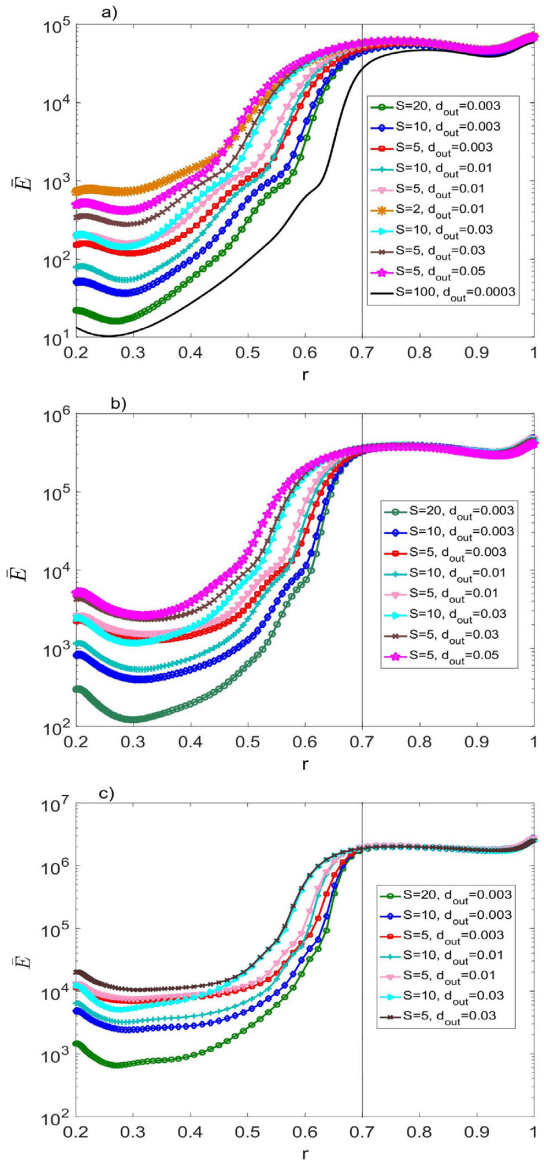

Figure 8. Kinetic energy profiles on a log scale for all the different S, $d_{\rm out}$ and for (a) $\mathrm{Ra_o} = 10^6$, (b) $\mathrm{Ra_o} = 10^7$, and (c) $\mathrm{Ra_o} = 10^8$.

a fairly wide range of values of the stiffness S, transition width $d_{\rm out}$, and Rayleigh number $\mathrm{Ra_o}$. Comparing Figs 8(a)–(c), we clearly see that increasing the input $\mathrm{Ra_o}$ increases the overall kinetic energy in the system (and accordingly, the amplitude of the Gaussian), which is expected since $\mathrm{Ra_o}$ controls the strength of the convection. Interestingly, varying S and $d_{\rm out}$ (at fixed $\mathrm{Ra_o}$) has very little effect on the kinetic energy within the CZ. This result is consistent with the notion that the turbulent intensity within the CZ only depends on its bulk Rayleigh number (Korre et al. 2017)

$$\mathrm{Ra_b} = \frac{\int_{r_t}^{r_o} \mathrm{Ra}(r) r^2 \, \mathrm{d}r}{\int_{r_t}^{r_o} r^2 \, \mathrm{d}r}, \tag{28}$$

which is roughly equal to $\mathrm{Ra_o}$ here since $\beta(r) \simeq -1$ for $r > r_t$ (see equation 13).

Korre et al. (2017) showed further that in spherical Rayleigh–Bénard convection bounded by impermeable walls, the mean kinetic

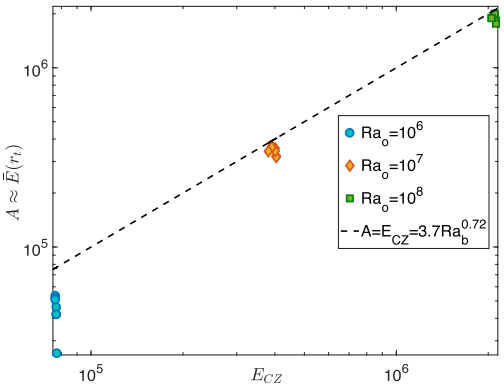

Figure 9. Plot of the extracted value of the amplitude of the Gaussian A against our model for the mean kinetic energy in the CZ (see equation 29).

energy of the convection zone $E_{\rm cz}$ scales as

$$E_{\rm cz} = 3.7 \mathrm{Ra_b^{0.72}}, \tag{29}$$

when its base is at $r_t = 0.7 r_o$ and $\mathrm{Pr} = 0.1$, which is also the case for the CZ in this paper. To verify whether this scaling also applies in a penetrative set-up and therefore could be used in a predictive model, we compare the total kinetic energy at r_t to the predicted value of $E_{\rm cz}$ in Fig. 9. The quantity $\bar{E}(r_t)$ is extracted from the simulations by fitting $f(r)$ to the data and assuming $\bar{E}(r_t) \simeq A$. We see that the predicted scaling works remarkably well for the more turbulent cases ($\mathrm{Ra_o} = 10^7$ and 10^8) and can therefore be used to obtain a good order-of-magnitude estimate of the amplitude of the turbulence present both within the CZ, as well as below the CZ–RZ interface through (23) provided a model for $\delta_{\rm G}$ is also available.

To construct such a model, we use a simple energetic argument. Assuming that a parcel travels a distance $\delta_{\rm en}$ from the base of the CZ adiabatically down to the point where its potential energy is equal to its initial kinetic energy, we can write

$$E_{\rm cz} = \delta_{\rm en} \frac{\mathrm{Ra_o}}{\mathrm{Pr}} \int_{0.7-\delta_{\rm en}}^{0.7} \beta(r) \, \mathrm{d}r \tag{30}$$

for the profile of $\beta(r)$ given in equation (13). Note that this assumes that the background temperature profile has not been modified too much by the overshooting motions; we could in principle obtain a more accurate estimate for $\delta_{\rm G}$ by using the actual stratification profile $\bar{N}^2 \mathrm{Pr}/\mathrm{Ra_o}$ computed from the simulations instead of the function $\beta(r)$ in the integrand. In practice, however, we verified that this does not make a substantial difference to the computed value of $\delta_{\rm en}$ in any of our simulations, where thermal mixing is always weak. Using $\beta(r)$ in the integrand on the other hand has definite advantages: the integral can be evaluated analytically so equation (30) becomes

$$E_{\rm cz} = \delta_{\rm en} \frac{\mathrm{Ra_o}}{\mathrm{Pr}} S d_{\rm in} \ln \left[\cosh \left(\frac{\delta_{\rm en}}{d_{\rm in}} \right) \right]. \tag{31}$$

Equation (31) can easily be solved numerically for $\delta_{\rm en}$, for any input S, $\mathrm{Ra_o}$, and $d_{\rm in}$.

In Fig. 10, we plot $\delta_{\rm G}$ against the energy-based theoretical prediction $\delta_{\rm en}$ for all available simulations. The quantity $\delta_{\rm G}$ was measured from the DNS simulations by fitting the Gaussian profile (23) to the total kinetic energy profile $\bar{E}(r)$ from r_t down to $r_t - \delta_\Theta$ (see Section 3), and all the results are reported in Table 1. We observe that all the points lie close to the straight line $\delta_{\rm G} = 1.2\delta_{\rm en}$ (dashed black line). This result is rather remarkable given that our input parameters span a fairly large region of parameter space, with

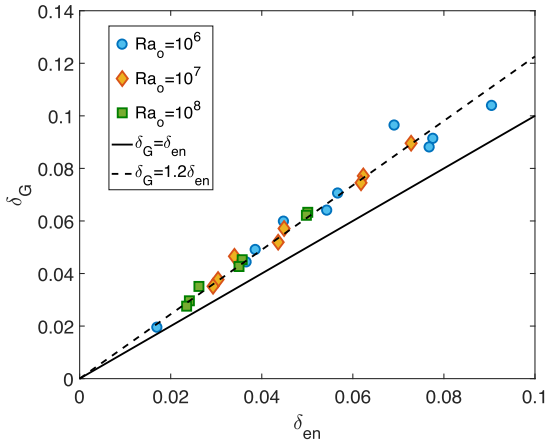

Figure 10. Plot of δ_{en} versus δ_G for all the cases where Ra_o has been used as reference.

a resulting δ_G ranging from ˜0.01 to ˜0.12. The result suggests that the physics of the energetic argument put forward is mostly correct. Note that the downflows originating from the convection zone obviously do not all have the same kinetic energy, so E_{cz} is merely an estimate of their mean, and δ_{en} is correspondingly merely an estimate of how far a typical eddy could overshoot. As a result, the prefactor relating δ_G to δ_{en} could have been any factor of the order of unity, but just happens to be 1.2 in this particular set of simulations. We expect this prefactor to vary somewhat if the Prandtl number varies dramatically, or if compressibility is taken into account.

While equation (31) does not have any analytical solutions in general, it has two limits of interest. When $\delta_{en} \ll d_{in}$, equation (31) becomes

$$E_{cz} \simeq \delta_{en} \frac{Ra_o}{Pr} S d_{in} \left(\frac{1}{2} \left(\frac{\delta_{en}}{d_{in}} \right)^2 \right), \tag{32}$$

leading to

$$\delta_{en} \simeq \left(\frac{2E_{cz} d_{out} Pr}{Ra_o} \right)^{1/3} \Rightarrow \delta_G \approx 1.2 \left(\frac{2E_{cz} d_{out} Pr}{Ra_o} \right)^{1/3} = 1.2 \left(\frac{2E_{cz} d_{in} Pr}{S Ra_o} \right)^{1/3}. \tag{33}$$

Physically speaking, this limit corresponds to the case where the downflows only sample the transition region below the CZ where $\beta(r)$ varies linearly with distance to r_t. As such, it is not surprising to find that δ_G in this case does not directly know about S, but only knows about the slope of $\beta(r)$. In Fig. 11(a), we plot the measured δ_G versus the transition width d_{out} along with the predicted line for δ_G as expressed in equation (33). We clearly see that our prediction works remarkably well for the cases where $\delta_G < d_{in}$.

In the opposite limit, when $\delta_{en} \gg d_{in}$,

$$E_{cz} \simeq \delta_{en} \frac{Ra_o}{Pr} S d_{in} \left(\frac{\delta_{en}}{d_{in}} \right), \tag{34}$$

leading to

$$\delta_{en} \simeq \left(\frac{E_{cz} Pr}{S Ra_o} \right)^{1/2} \Rightarrow \delta_G \approx 1.2 \left(\frac{E_{cz} Pr}{S Ra_o} \right)^{1/2}. \tag{35}$$

In this limit the downflows penetrate down to the region where $\beta(r) \simeq S$, so it is not surprising to see that δ_G depends on S, but is independent of d_{out}. Fig. 11(b) shows the measured δ_G against the stiffness parameter S along with the scaling given in equation (35). We find that the scaling law $S^{-1/2}$ works for the simulations in which $\delta_G > d_{in}$, but is off by a constant factor. This is not too surprising since the expansion used to obtain equation (35) is technically valid only in the limit $(\delta_{en}/d_{in}) \to \infty$, which does not hold true for any of our simulations where δ_G is fairly close to d_{in}.

Ultimately, we see that δ_G is either proportional to $S^{-1/3}$ or to $S^{-1/2}$, implying that it decreases with increasing S in both limits. This is in agreement with the naive expectation that turbulent fluid motions generated in the CZ have a harder time penetrating deeply into a more strongly stratified RZ. These scalings are quite different from the ones proposed by Zahn (1991) and Hurlburt et al. (1994), which both argue for a penetration depth (i.e. the depth of the adiabatically stratified layer) scaling as S^{-1}, and an overshoot depth (the depth of their thermal adjustment layer) scaling as $S^{-1/4}$. The difference between their theory and our results is relatively easy to understand, however. To start with, their model set-up is quite different from ours, relying on changes in the thermal conductivity to drive the transition from a radiative to a convective environment, whereas we produce this transition by effectively adding a heating source (see Section 2). Since their theoretical predictions fundamentally rely on the changes in thermal conductivity, it is not surprising that they would be at odds with our own scalings. Furthermore, their S^{-1} scaling relies on the existence of an adiabatic penetrative layer, and their $S^{-1/4}$ scaling relies on an exponentially damped overshoot. Neither of these dynamics are seen here. Note also that Rogers & Glatzmaier (2005) presented the results of 2D anelastic simulations of penetrative and overshooting convection, where they confirmed the S^{-1} scaling in the penetrative limit, but report on a much shallower scaling law $\sim S^{-0.04}$ in the moderate- and high-S non-penetrative limit. While their definition of S differs somewhat from that of Hurlburt et al. (1994), that difference cannot fully explain the rather large discrepancy in observed scaling with S. Instead, clues to the possible origin of this discrepancy might lie in the applied thermal boundary conditions: Rogers & Glatzmaier (2005) use isothermal boundary conditions, and state that *'In simulations in which a constant heat flux boundary condition is used at the top, the scaling relation at moderate S values is not as shallow'*. Our findings then do not contradict any of these results.

Finally, we note that δ_G counterintuitively decreases with increasing Ra_o in both of these limits. Indeed, one would expect that the increase in the turbulent convective velocities associated with a higher Ra_o would lead to deeper overshooting into the RZ. However, the background stratification of the deep RZ in our model set-up scales like $\bar{N}^2 \simeq S Ra_o/Pr$ that increases with increasing Ra_o for fixed values of S. We therefore see that this second effect dominates the system dynamics, leading to a shallower – not deeper – δ_G as Ra_o increases.

5 THERMAL MIXING IN THE RZ

In this section, we focus on quantifying the properties and dependence on input parameters of the regime of partial thermal mixing in the RZ. Fig. 12(a) shows $\bar{\Theta}_{down}$, and $\bar{\Theta}$, as defined earlier, for the simulation with $S = 5$, $d_{out} = 0.003$, and $Ra_o = 10^7$ (Case 11, Table 1) analysed in Section 3, along with a more laminar case of $Ra_o = 10^6$ (Case 2, Table 1) and a more turbulent case of $Ra_o = 10^8$ (Case 19, Table 1). Fig. 12(b) shows the corresponding buoyancy frequency profiles, and Fig. 12(c) shows the associated turbulent temperature flux (see below for its definition and discussion).

Within the CZ, we find that $\bar{N}^2$ is closer to 0 (and correspondingly that $\bar{\Theta}$ follows Θ_{ad} more closely) for larger Ra_o. This is to be

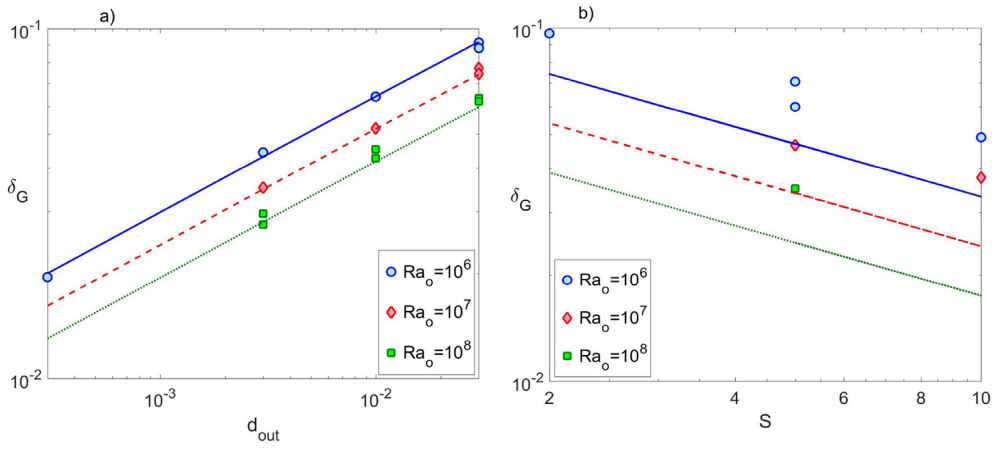

Figure 11. Plot of the measured δ_G against (a) the transition width d_{out}, and (b) the stiffness parameter S. In (a), only those simulations for which $\delta_G < \delta_{in}$ are shown. Also shown is the predicted scaling law for δ_{en} given in equation (33). In (b), only those simulations for which $\delta_G > \delta_{in}$ are shown. Also shown is the predicted scaling law for δ_{en} given in equation (35).

expected since a more turbulent convection zone is more efficient in driving the mean temperature towards an adiabatic state. Meanwhile in the radiative region, we recover the same overall behaviour for $\bar{N}^2$, $\bar{\Theta}_{down}$, and $\bar{\Theta}$ that was already observed in the reference simulation: mixing is not strong enough to cause an extension of the convection zone, but does smooth out the mean stratification down to a depth $\sim\delta_\Theta$ below the base of the CZ. We also see that δ_Θ decreases with increasing $\mathrm{Ra_o}$ (and same is true for δ_u), as shown in Table 1. This trend mirrors the corresponding decrease in δ_G with increasing Rayleigh number discussed in Section 4, which was attributed to the increasing stratification of the RZ. Since δ_Θ continues to be a good proxy for the depth of the partially thermally mixed region (see Fig. 12b), our findings therefore imply that the latter becomes shallower with increasing $\mathrm{Ra_o}$.

More generally, we have found that δ_u, δ_Θ, and δ_G are all very closely related to one another across all of our simulations and can easily be predicted from the energy-based length-scale δ_{en} proposed in Section 4. Indeed, as shown in Fig. 13, we find that $\delta_u \simeq \delta_\Theta \simeq 2.9\delta_{en}$. In other words, the energy-based argument proposed in Section 4 applies equally well to predict the neutral buoyancy point and the stopping depth of individual (strong) downflows, albeit with a somewhat larger prefactor. This provides a very simple way of estimating the depth of the partially thermally mixed region below the base of the convection zone simply from knowledge of the model parameters.

A complete model for thermal mixing by convective overshoot requires a quantitative understanding of the strength of such mixing, i.e. of the turbulent heat flux. In this particular model set-up, the turbulent heat flux can easily be measured once the system is in a statistically stationary state. Indeed, taking the horizontal average of the thermal energy equation (10) in that state, integrating it once, and applying the boundary condition at r_i, we find that

$$\bar{F}_T \equiv \overline{u_r \Theta} = \frac{1}{\mathrm{Pr}} \frac{\partial \bar{\Theta}}{\partial r}, \tag{36}$$

or in other words, that the sum of the turbulent and diffusive heat fluxes associated with the temperature perturbation $\bar{\Theta}$ must be zero. This is consistent with our assumption that the total flux through the system is fixed. We then have

$$\bar{F}_T = \frac{1}{\mathrm{Pr}} \left(\frac{\bar{N}^2 \mathrm{Pr}}{\mathrm{Ra_o}} - \beta(r) \right), \tag{37}$$

so the turbulent temperature flux $\bar{F}_T$ can easily be visualized on Fig. 12(b) as the (signed) difference between the dashed line and the solid line (times Pr^{-1}). It is shown, for better clarity, in Fig. 12(c) for the same runs.

As expected, the temperature flux is generally negative in the radiative zone and positive in the convection zone. It almost always changes sign very close to the radius where $\bar{N}^2$ changes sign. In none of the simulations do we see the formation of an *extended* stably stratified region subject to substantial positive non-local convective fluxes of the kind reported by Käpylä et al. (2017), who called such a layer a 'Deardorff layer' following Deardorff (1966) and Brandenburg (2016). This difference between our simulations and theirs is probably due to two complementary effects. Käpylä et al. (2017) ran fully compressible simulations that more realistically capture the asymmetry between weak warm upflows and strong cold downflows than our Boussinesq set-up. This asymmetry promotes non-local heat transport by the plumes, allowing the strongest cold downflows to penetrate more coherently and more deeply into the RZ than they would otherwise before warming up. Compressibility is however not a sufficient condition for the formation of a significant Deardorff layer, since none were seen in the compressible simulations of Brummell et al. (2002) or Pratt et al. (2017). Käpylä et al. (2017) explain this, showing that the Deardorff layer is almost absent if the thermal diffusivity profile (or equivalently, the background radiative temperature profile) is fixed and varies abruptly with depth, which is indeed the case in the simulations of Brummell et al. (2002). In our numerical set-up, which uses the Boussinesq approximation, the asymmetry between upflows and downflows is weak, induced only by the spherical geometry and the boundary conditions. In addition, most of our simulations were run with a transition steepness set by taking $d_{out} = 0.003$, which is very sharp (e.g. see Fig. 12). We therefore should not expect to see the formation of a Deardorff layer in these cases. We can, however, detect the existence of one in the largest d_{out} runs (i.e. when $d_{out} = 0.03$; see Fig. 14) but it remains very shallow. As such, our simulations cannot really probe the dynamics of the Deardorff layer even though we might expect that one should be present in the Sun.

The magnitude of the turbulent flux below the CZ increases with $\mathrm{Ra_o}$, as seen in Fig. 12(c), even though the depth of the mixed layer concurrently decreases. This is not surprising since the rms velocity

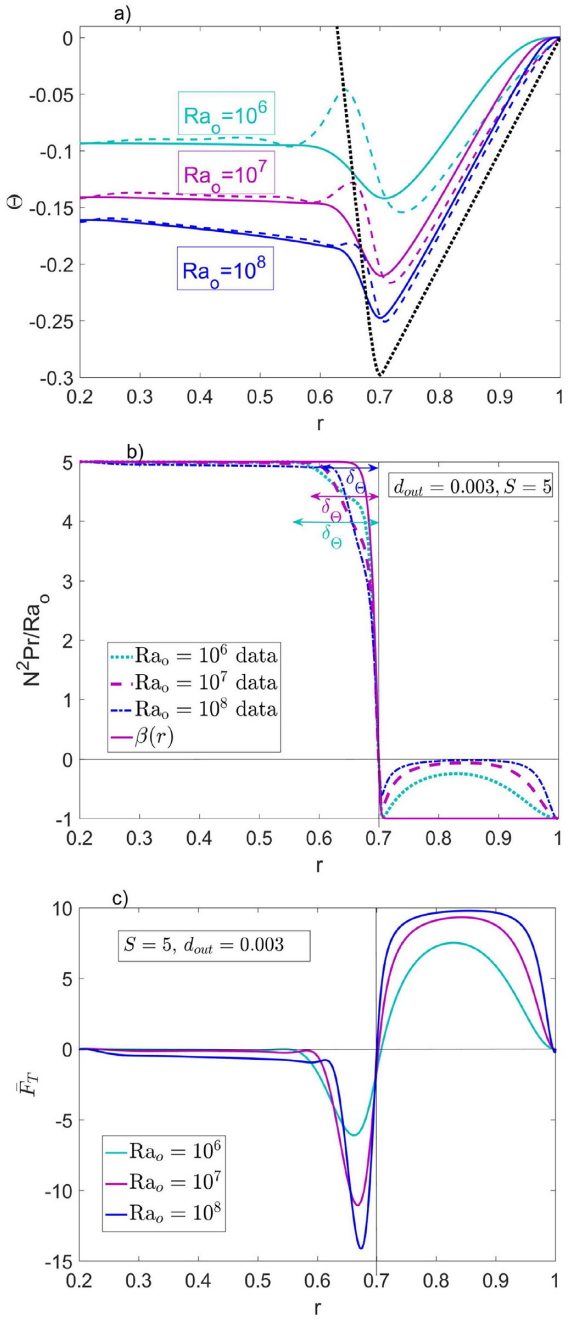

Figure 12. (a) Plot of the temperature perturbations (where the solid lines correspond to $\bar{\Theta}$ and the dashed lines correspond to $\bar{\Theta}_{\rm down}$) along with the respective adiabatic one (dotted black line), (b) plot of $\bar{N}^2(r)\mathrm{Pr}/\mathrm{Ra_o}$ along with the respective $N^2_{\rm rad}(r)\mathrm{Pr}/\mathrm{Ra_o}$, and (c) plot of the fluxes $\bar{F}_T$, for $S = 5$, $d_{\rm out} = 0.003$, and three different $\mathrm{Ra_o}$.

of the downflows increases with $\mathrm{Ra_o}$ (see equation 29). However, the increase of $\bar{F}_T$ with Rayleigh number is not particularly pronounced, perhaps scaling as $\bar{F}_T \sim \mathrm{Ra_o}^{0.18}$. Within the scope of the simulations shown here, we see that increasing $\mathrm{Ra_o}$ by a factor of 100 only increases the peak value of $|\bar{F}_T|$ by a factor of about 2.2 in the RZ. This shows that the turbulent flux itself does not scale as steeply as the rms velocity (which would lead to $\bar{F}_T \sim \mathrm{Ra_o}^{0.36}$), implying in turn that the amplitude of the temperature fluctuations must decrease with increasing $\mathrm{Ra_o}$. This can, in fact, easily be verified in Fig. 12(a), which shows that the profiles of $\bar{\Theta}$, and $\bar{\Theta}_{\rm down}$ are much closer to one another at $\mathrm{Ra_o} = 10^8$ than at $\mathrm{Ra_o} = 10^6$. This result can be explained by noting that turbulence plays an increasingly dominant role at larger Rayleigh number and has a tendency to homogenize the temperature between upflows and downflows. Given the weak dependence on $\mathrm{Ra_o}$, the range of available simulations is unfortunately not large enough to extract a reliable scaling law between $\bar{F}_T$ and $\mathrm{Ra_o}$ – the latter could be a power law (in which case the power would be of the order of 0.18, as mentioned earlier), but could just as well be logarithmic, or take some other form. As a result, we defer any prediction on the scaling of $\bar{F}_T$ with $\mathrm{Ra_o}$ to future work. Nevertheless, our results point to the crucial importance of accounting for the turbulent mixing between upflows and downflows when modelling mixing by overshooting convection, something that had rarely been taken into account in previous plume models of overshoot (Shaviv & Salpeter 1973; Schmitt et al. 1984) until the work of Rempel (2004).

Finally, we explore the dependence of thermal mixing on S and $d_{\rm out}$ in Fig. 14(a), which shows $\bar{N}^2(r)\mathrm{Pr}/\mathrm{Ra_o}$ and $N^2_{\rm rad}(r)\mathrm{Pr}/\mathrm{Ra_o} = \beta(r)$ for our typical simulation of $S = 5$, $d_{\rm out} = 0.003$, and $\mathrm{Ra_o} = 10^7$ (case 11, Table 1) along with one from a simulation with the same $S = 5$ and $\mathrm{Ra_o}$ but a larger $d_{\rm out} = 0.03$ (shallower transition; case 16, Table 1), and one with the same $d_{\rm out} = 0.003$ and $\mathrm{Ra_o}$, but a larger $S = 10$ (stiffer case; case 12, Table 1). Fig. 14(b) shows the corresponding turbulent fluxes for the same simulations. We see that increasing S at fixed $d_{\rm out}$ varies δ_Θ a little (so the partially mixed layer below the CZ is somewhat shallower), but the magnitude of the turbulent flux is hardly affected. Increasing $d_{\rm out}$ at fixed S on the other hand has a much larger effect on δ_Θ (which increases significantly), and on the fluxes (which decrease by about 25 per cent). This shows the importance of smooth versus abrupt transitions in $\beta(r)$, but we have not yet been able to construct a quantitative model to explain these results.

6 SUMMARY AND DISCUSSION

6.1 Summary

In this paper, we have presented a series of numerical experiments designed to quantify the interaction between a convective zone and an underlying stably stratified zone, in a spherical geometry and within the context of the Boussinesq approximation. In order to mimic the stellar case, we have used a fixed-flux inner boundary condition at a radius located somewhat above the nuclear burning region, and a fixed-temperature outer boundary condition. For simplicity, all the diffusivities as well as gravity are held constant in the domain, and so is the adiabatic temperature gradient. As a result, a heating source must be invoked in the vicinity of the radiative–convective interface to ensure that the lower part of the domain is indeed stably stratified, while the upper part of the domain is convectively unstable. The selected radial distribution and amplitude of the heating source sets the radiative temperature gradients in the radiative and convective zones, respectively, and can be adjusted to create stable and unstable regions with varying relative stability (quantified through the non-dimensional stiffness parameter S), as well as steeper or shallower transitions between the two (quantified through the non-dimensional transition width $d_{\rm out}$): see Section 2. For simplicity, the overall geometry of the system was fixed to mimic the solar case (with the radiative–convective interface located at $r_{\rm t} = 0.7r_{\rm o}$), and we also fixed the Prandtl number $\mathrm{Pr} = \nu/\kappa = 0.1$ in all of our simulations. The parameters varied were S and $d_{\rm out}$ as well as the global Rayleigh number $\mathrm{Ra_o}$

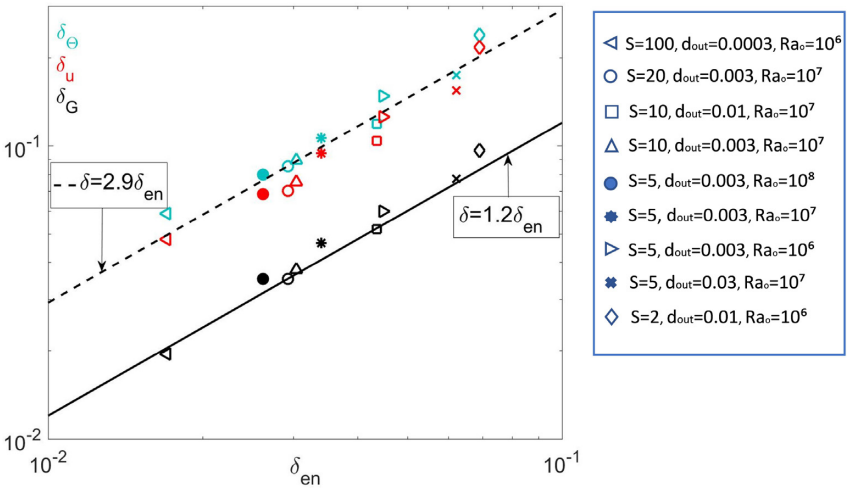

Figure 13. Comparison of δ_u, δ_Θ, and δ_G against the estimated δ_{en} for the simulations indicated on the legend. Also shown are the best fit to the data, namely $1.2\delta_{en}$ for δ_G and $2.9\delta_{en}$ for δ_u and δ_Θ.

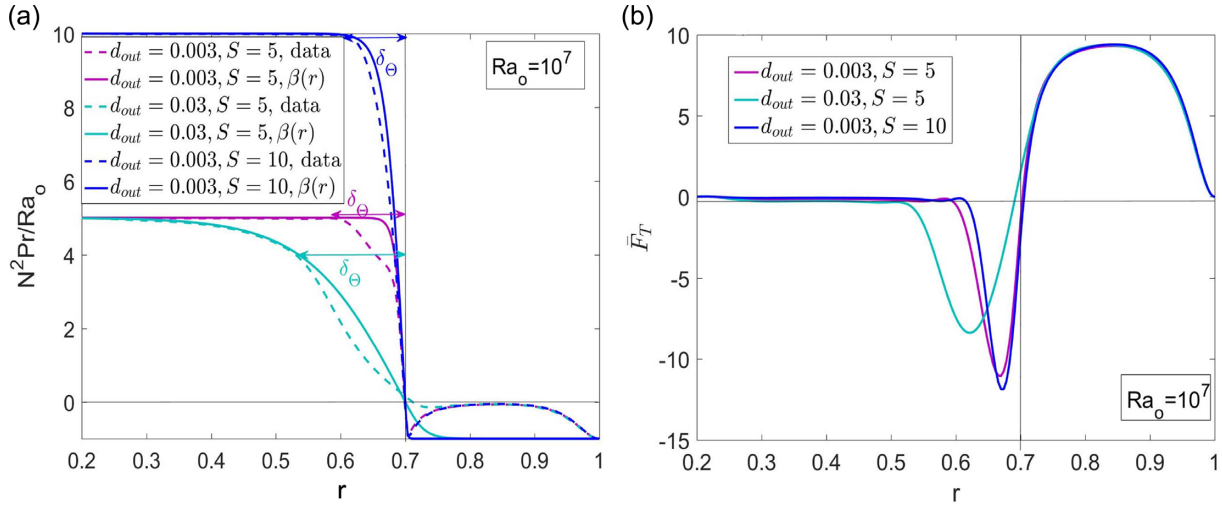

Figure 14. (a) Comparison of $\bar{N}^2(r)\mathrm{Pr}/\mathrm{Ra_o}$ with the corresponding background, $\beta(r)$, for simulations with $\mathrm{Ra_o} = 10^7$, two different values of S (5 and 10), and two different values of d_{out} (0.003 and 0.03). (b) Corresponding turbulent temperature fluxes for the same simulations.

(defined in equation 11). Increasing $\mathrm{Ra_o}$ is therefore equivalent to reducing the viscosity and thermal diffusivity concurrently. We explored simulations with $\mathrm{Ra_o}$ ranging from 10^6 to 10^8. Note for comparison that $\mathrm{Pr} \sim 10^{-6}$ and $\mathrm{Ra_o} \gg 10^{20}$ in the Sun, so none of the simulations should be used to *directly* infer properties of the overshooting convective motions. Instead, we merely seek to understand how the properties of the radiative–convective interface *scale* with input parameters, to later attempt an extrapolation of the results to the solar case (while always maintaining some degree of healthy skepticism).

Our simulations all share the same characteristics. We found as in Korre et al. (2017) that at fixed aspect ratio and fixed Pr, the mean kinetic energy in the CZ, called E_{cz}, scales as $\mathrm{Ra_b^{0.72}}$ (see equation 29), where $\mathrm{Ra_b}$ is the volume-averaged Rayleigh number within the CZ (see equation 28), which in this work is quite close to $\mathrm{Ra_o}$. The total kinetic energy of fluid motions decays below the radiative–convective interface as a Gaussian function of the distance to r_t (see equation 23) whose width δ_G can be predicted from first principles using a simple energy argument (aside from a constant of the order of unity). Indeed, assuming that an average downflow travels a distance δ_{en} adiabatically from the base of the convection zone until its potential energy equals its estimated initial kinetic energy E_{cz}, we can compute δ_{en} by solving equation (31). We then showed that, for all available simulations, $\delta_G \simeq 1.2\delta_{en}$. Through this equation, we can then quantify how δ_G varies with both the stiffness and steepness of the background stratification profile as well as with the input Rayleigh number.

We also looked more specifically at how far the *strongest* downflows penetrate into the RZ, by computing the correlation function $C(\delta)$ between the radial velocity at r_t and a distance δ away from it. We found that these strong downflows stop at a distance $\delta_u \simeq 2.9\delta_{en}$ from the base of the convection zone, for any S, d_{out} and $\mathrm{Ra_o}$. This distance δ_u, computed as the first zero of $C(\delta)$, also turns out to correspond to the level of neutral buoyancy for the downflows δ_Θ. The strict correlation discovered between δ_u, δ_G, and δ_{en} therefore strongly suggests that the simple energetic argument put forward is sufficient to characterize the dynamics of the overshooting plumes.

We found that the region between $r_t - \delta_u$ and r_t is partially thermally mixed (at these values of the Rayleigh number), resulting in an adjusted buoyancy frequency profile substantially smoother

than that of the imposed background. However, we did not see any actual penetration in the traditional definition of the extension of the CZ into the RZ (e.g. Zahn 1991; Hurlburt et al. 1994). This is because the turbulent temperature flux $\bar{F}_T$ induced by overshooting motions in the RZ remains moderate in all the simulations. We found that it is independent of S and only scales weakly with Rayleigh number (increasing by a factor of about two when $\mathrm{Ra_o}$ increases by a factor of 100), suggesting either a very weak power law ($\bar{F}_T \propto \mathrm{Ra_o}^{0.18}$) or a logarithmic dependence on $\mathrm{Ra_o}$.

Finally, below $r_\mathrm{t} - \delta_\mathrm{u}$ the nature of the system dynamics clearly change. The turbulent temperature flux becomes negligible, and the kinetic energy profile is no longer Gaussian, but appears closer to exponential. While weak fluid motions are present, they appear to be more related to the 'damped tail' of linearly unstable convective modes (in the sense described by Freytag et al. 1996, for instance) rather than to internal gravity waves.

6.2 Comparison with previous numerical experiments

As discussed in Section 1, there have been quite a few numerical investigations of the dynamics of overshooting and penetrative convection to date. In what follows, we focus on the ones that address the question of overshoot under a convective zone (sometimes referred to as 'undershoot', although we prefer not to use that terminology), rather than above it. These include (among others) the 2D fully compressible simulations of Hurlburt et al. (1986), Hurlburt et al. (1994), Freytag et al. (1996), and Pratt et al. (2017), the 3D fully compressible simulations of Brummell et al. (2002), Singh et al. (1995; see also Singh et al. 1998; Saikia et al. 2000), Käpylä et al. (2017), the 2D anelastic simulations of Rogers & Glatzmaier (2005; see also Rogers, Glatzmaier & Jones 2006), and the 3D ones of Brun et al. (2017).

Several general conclusions can be drawn from comparing the outcome of these simulations to one another and to ours. First and foremost is that penetrative convection in the strict definition of the term (i.e. the extension of the convection zone substantially beyond the threshold for linear instability) had so far not been observed in fully turbulent 3D simulations (Brummell et al. 2002; Brun et al. 2017; Käpylä et al. 2017), and this continues to be the case here. As reviewed in Section 1, the fact that penetration is seen in 2D at sufficiently low values of S (e.g. Rogers & Glatzmaier 2005) and in very laminar 3D simulations (e.g. Saikia et al. 2000) can be attributed to the artificially large geometric filling factor of 2D plumes versus 3D plumes (Brummell et al. 2002; Rempel 2004). However, none of the existing 3D simulations (including ours) reach particularly high values of the Rayleigh number. Hence, whether this result will continue to hold when progress in supercomputing allows us to simulate convection at much higher Rayleigh numbers remains to be determined (see below for more on this point).

A second common point between (almost) all simulations is that the kinetic energy of vertical motions within the downflows drops substantially within the CZ as they approach the RZ from above, owing to their lateral deflection, even in low stiffness cases. As a result, the dominant contribution to the total kinetic energy within the RZ is from horizontal flows. While this may superficially seem at odds with the standard mental picture one may have of overshooting plumes, note that most of the vertical transport is still carried out by the strongest, most-concentrated downflowing motions, as was described in other simulations, e.g. Brummell et al. (2002) and Pratt et al. (2017), but the content of these strongest plumes (heat, chemical species) is then advected (and mixed) laterally by turbulent horizontal flows. Precisely how strong these concentrated downflows can get (for given Rayleigh and Prandtl numbers in the CZ) depends on the dimensionality of the simulations and on the compressibility of the fluid (Boussinesq versus anelastic versus fully compressible). Since the strength and depth of the downflows control other RZ processes, such as the generation of gravity waves or the formation of a Deardorff layer, for instance, it is not surprising to see that the latter are strongly model-dependent, present in some simulations, absent in others.

A third common point between all simulations is that the depth of the turbulent overshooting layer (as measured by looking at either the kinetic energy profile or the kinetic energy flux below the base of the CZ) does seem to decrease with increasing stiffness S, which is an intuitive result. What differs however is the measured scaling law relating this depth to S. Hurlburt et al. (1994) and Brummell et al. (2002) both ran DNS of overshooting convection in 2D and 3D, respectively, where the radiative–convective transition is caused by a sudden change in the thermal conductivity. They both state that their results are consistent with estimates based on a variant of Zahn's theory (Zahn 1991), which predicts that the overshooting depth should scale as $\sim S^{-1/4}$ when the total flux through the system is fixed. Our findings are not directly comparable to those reported in Zahn (1991), who only considered two distinct regimes: a very high Pe regime and a very low Pe regime. The high Pe regime is associated with pure penetrative convection while in the low Pe regime, diffusion dominates and leads to a thermal boundary layer associated with overshooting. Instead, the Péclet numbers estimated in the overshoot region, and shown in Table 1 range from about 0.5 to approximately 10. Our reported values of $\mathrm{Pe_{ov}}$ are clearly neither in the very low Pe regime nor in the very large Pe regime, thus our findings cannot be directly compared to the regimes found in Zahn (1991). Rogers & Glatzmaier (2005) presented 2D anelastic simulations with fixed temperature boundary conditions, where the radiative–convective transition is also caused by a sudden change in the thermal conductivity and found a much shallower scaling law $\sim S^{-0.04}$. Meanwhile, in our Boussinesq 3D fixed flux DNS, where the transition is driven by the existence of a heating source around r_t, we find somewhat steeper scaling laws, with $\sim S^{-1/3}$ or $\sim S^{-1/2}$ depending on whether the background radiative temperature gradient is shallower or steeper, respectively. We believe that the observed difference in the scaling laws reported in these various papers is more likely to be due to the differences in boundary conditions or model set-up used rather than compressibility, but this should be verified in future work. It would be interesting, for instance, to run a comparative study of overshooting and penetrative convection in various systems that all have the same background profile of N^2, but that are driven in different ways (i.e. by varying the diffusivities, or the equation of state, or using a heating function, for instance).

In any case, gaining a better understanding of the scaling of the overshoot depth with S is arguably less important than constraining its scaling with the Rayleigh number, since S is not expected to be too large in stars. $\mathrm{Ra_o}$, on the other hand, needs to be increased by more than 10 orders of magnitude to reach the stellar regime. Not many studies have systematically looked into this problem. The work of Brummell et al. (2002) seems to suggest (see their Section 3.7) the approximate scaling $\delta \sim \mathrm{Ra}^{-0.25}$. In Rogers & Glatzmaier (2005), the situation is complicated by the fact that the measured scalings with Rayleigh number appear to depend sensitively on S: in the less stiff cases, the overshooting layer depth increases with Rayleigh number, but the opposite is true for stiffer cases. The simplicity of our simulations, however, easily allows us to vary $\mathrm{Ra_o}$ independently of all other parameters, and we find that $\delta_\mathrm{G} \sim \mathrm{Ra_o}^{-0.09}$

in the case where the transition is steep, and $\delta_G \sim \mathrm{Ra}_o^{-0.14}$ when it is shallow. In both cases the overshoot depth therefore decreases with Ra_o at fixed S as discussed in Section 4 (see equations 33 and 35, using $E_{cz} \sim \mathrm{Ra}_o^{0.72}$), although the actual power law is quite shallow.

Finally, we note that very few studies, to our knowledge, really looked into the actual spatial variation of the kinetic energy profile with depth (which is a good proxy for the variation of the mixing coefficient with depth, see below). Freytag et al. (1996) were the first to clearly state that their simulations show an exponential decay of the rms velocities with depth below the convection zone. They showed that this profile is consistent with these velocities being the stable exponentially decaying tail of the linearly unstable convective modes. Unfortunately, this also demonstrates that their simulations cannot be in the turbulent regime, a notion that is consistent with a simple visual inspection of their fig. 2–5. By contrast, our simulations are quite turbulent down to about $r_t - \delta_u$ (although obviously, the $\mathrm{Ra}_o = 10^6$ cases are somewhat less turbulent than the $\mathrm{Ra}_o = 10^8$ ones in the first place). We find that the kinetic energy profile is Gaussian instead of exponential in that region, and only becomes exponential once the fluid motions are sufficiently slow for all non-linearities to be negligible.

6.3 A prescription for mixing by overshoot

In this section, everything is now presented and discussed in dimensional terms (assuming cgs units). All the variables are now implicitly dimensional. Our numerical results have led us to suggest a very simple Gaussian model for the kinetic energy profile below the base of the convection zone given by

$$E(r) = E_{cz} \exp\left(-\frac{(r-r_t)^2}{2\delta_G^2}\right), \tag{38}$$

where E_{cz} is the typical kinetic energy of fluid motions within the convection zone (i.e. somewhere within the bulk of the zone). This quantity can, for instance, be determined from mixing length theory in a stellar evolution code, or from equation (29) in more idealized Boussinesq set-ups (recalling that the prefactor could depend on the Prandtl number and on the aspect ratio of the convective region). The length-scale δ_G, on the other hand, can be estimated by using the energy-based length-scale δ_{en} discussed in Section 4 (see equation 30), with $\delta_G \simeq \delta_{en}$. A factor of unity relating the two is left unspecified here and may weakly depend on the Prandtl number and on compressibility. Dimensionally speaking, the length-scale δ_{en} can be found by solving the equation

$$\frac{1}{2}v_{cz}^2 = -\delta_{en}\int_{r_t-\delta_{en}}^{r_t} \frac{g}{H_p}\left(\nabla - \nabla_{ad}\right) \mathrm{d}r, \tag{39}$$

where v_{cz} is the convective velocity in the bulk of the convection zone, g is the local gravity, $\nabla = \partial \ln T/\partial \ln p$ is the radiative temperature gradient, $\nabla_{ad} = (\partial \ln T/\partial \ln p)_{ad}$ is the adiabatic temperature gradient, and H_p is the pressure scale height. With this formula, the computation of the depth δ_G only depends on the local temperature gradient as well as standard variables returned by stellar evolution codes, rather than the manner in which this temperature gradient (and the CZ–RZ transition) is actually generated. Note that this energy-based argument for estimating the overshoot depth is ultimately quite standard; it recovers, for instance, that of Christensen–Dalsgaard et al. (2011; see their equation 18) if $\nabla - \nabla_{ad}$ is taken to be approximately constant below the base of the convection zone, in which case δ_{en} satisfies

$$\frac{\delta_{en}}{H_p} = \left(\frac{v_{cz}^2}{2gH_p|\nabla - \nabla_{ad}|}\right)^{1/2}. \tag{40}$$

If, on the other hand, $\nabla - \nabla_{ad}$ is assumed to vary linearly with depth below the CZ, with $\nabla - \nabla_{ad} \simeq \eta(r - r_t)$, then

$$\frac{\delta_{en}}{H_p} = \left(\frac{v_{cz}^2}{gH_p^2\eta}\right)^{1/3}. \tag{41}$$

Note that if convection is very efficient and transports the majority of the stellar luminosity, then equations (39)–(41) can be expressed in terms of the convective flux (instead of the convective velocity). To do so, we assume that the two are related according to

$$F_{conv} = \frac{4\rho c_p T}{g\delta l_m} v_{cz}^3, \tag{42}$$

where $\delta = \frac{\partial \ln \rho}{\partial \ln T}$, c_p is the specific heat at constant pressure and l_m is the mixing length (see e.g. Kippenhahn & Weigert 1990; Chapter 7). Under the conditions for which this relationship holds, then we would have

$$\delta_{en} \propto F_{conv}^{1/3} \tag{43}$$

if $\nabla - \nabla_{ad}$ is almost constant below the CZ and

$$\delta_{en} \propto F_{conv}^{2/9} \tag{44}$$

if $\nabla - \nabla_{ad}$ increases linearly away from the radiative–convective interface.

From the kinetic energy profile (38), we can then form a diffusion coefficient to model compositional mixing by overshooting motions

$$D_{ov}(r) = D_{cz} \exp\left(-\frac{(r-r_t)^2}{2\delta_G^2}\right), \tag{45}$$

assuming that $D_{ov} \propto v_{cz}^2 \tau_{cz}$ as in Freytag et al. (1996), where τ_{cz} is some convective turnover time-scale just above the base of the convection zone.

In order to apply equation (41) to the Sun, we extract all the relevant quantities from the interface between the interior radiation zone and convective envelope of a 1 solar mass Main-Sequence model computed with MESA[1] (Paxton et al. 2011, 2013). We find that $v_{cz} \simeq 6000\,\mathrm{cm\,s^{-1}}$ in the bulk of the convection zone, and $g \simeq 50\,000\,\mathrm{cm\,s^{-2}}$, $H_p \simeq 5 \times 10^9$ cm, and $\eta \simeq 10^{-10}\,\mathrm{cm^{-1}}$ near the interface, leading to $\delta_{en}/H_p \simeq 0.006$. Similar calculations made at the interface between the interior convective zone and radiative envelope of a 2 solar mass Main-Sequence model yield $v_{cz} \simeq 7000\,\mathrm{cm\,s^{-1}}$, $g \simeq 200\,000\,\mathrm{cm\,s^{-2}}$, $H_p \simeq 5 \times 10^9$ cm, and $\eta \simeq 10^{-11}\,\mathrm{cm^{-1}}$, leading to $\delta_{en}/H_p \simeq 0.01$. In both cases, δ_{en} (and by definition δ_G) is quite a small fraction of a pressure scale height and would result in much shallower predictions for the depth of the overshoot-mixed layer than what is commonly assumed in stellar evolution models [e.g. from the model of Herwig (2000) with $f \simeq 0.1H_p$]. Even shallower predictions would be obtained using values of v_{cz} taken closer to the edge of the convective region. Whether overshoot is, in fact, as shallow as predicted in real stars remains to be determined. As discussed in Section 1, it is not unlikely that moving beyond the Boussinesq approximation could result in a somewhat larger overshoot depth than what we currently see in the simulations, simply because of the pressure-induced enhancement

[1] Version 6794.

of the asymmetry between narrow downflows and broad upflows. In addition, since δ_{en} depends sensitively on v_{cz}, the reliability of our model predictions effectively depends on the reliability of mixing-length theory (Böhm-Vitense 1958; Cox & Giuli 1968) in estimating the typical velocities of convective motions deep within a star. Asteroseismology will hopefully help constrain the latter in the coming years. Nevertheless, it is difficult to see how the overshoot depth could vary substantially away from δ_{en} predicted using the simple energy balance argument given in equation (39). It is worth remembering at this point that Zahn's original models (Zahn 1991; Hurlburt et al. 1994) also predict a very shallow overshoot layer (in the strict definition of the term) – but that layer only starts beyond a thermally mixed penetration layer that can be much larger (at least for the smaller values of S). As such, our findings (in terms of strict overshoot) are not inconsistent with observations of substantial mixing beyond the edge of a convective region (Liu et al. 2014; Deheuvels et al. 2016), as long as these observations are interpreted as evidence for penetration (rather than overshoot).

As discussed in Section 5, estimating the amount of *thermal* mixing below the CZ (and therefore quantifying penetration) is much more complicated, as this requires knowledge not only of the velocities, but also of the typical temperature fluctuations associated with upflows and downflows relative to the background profile, which in turn depend on the relative importance of both small-scale horizontal turbulent mixing and thermal diffusion, as well as the global thermal equilibrium. This cannot be done using simple local energetic/thermal balance arguments, and it seems that the only way forward is to analyse the results of numerical simulations to create an empirical model for the heat flux. The problem with this approach, however, is that it is very sensitive to the model set-up used (i.e. compressible versus anelastic versus Boussinesq, 2D versus 3D, boundary conditions, method for generating the CZ–RZ transition), as noted by the rather vast discrepancies in results obtained in the numerical experiments discussed in Section 1. Further work will be required to better understand the causes of this sensitivity and to determine what results can and cannot be carried over (qualitatively and quantitatively) from idealized models to more realistic stellar environments.

Within the scope of numerical simulations run in the same set-up as ours, we could tentatively extrapolate our results to estimate the magnitude of the turbulent temperature flux $\bar{F}_T$ induced below r_t by the convective motions. However, we found that the latter only varies very weakly with Rayleigh number to the extent that we are unable to propose any definite model for the former. If a power law is assumed, then our results suggest that $\bar{F}_T \propto \mathrm{Ra}_o^{0.18}$. If that scaling holds, we predict that it may be possible to see convective penetration in Boussinesq convection at higher Rayleigh numbers (holding the Prandtl number constant). Indeed, taking our reference simulation ($\mathrm{Pr} = 0.1$, $S = 5$, $d_{out} = 0.003$, $\mathrm{Ra}_o = 10^7$) for instance, we see that the turbulent flux would have to be about five times larger than it is to drive the profile of $\bar{N}^2$ towards an adiabat below the base of the CZ, which would require an input Rayleigh number (defined as in equation 11) of the order of about 10^{11}. Another way of looking at the problem is to estimate how the Péclet number varies with Ra_o. Given that $\mathrm{Pe}_{ov} = u_{rms}\delta_G \mathrm{Pr}$, where $u_{rms} \propto \mathrm{Ra}_b^{0.36}$ (see equation 29) and $\delta_G \approx \delta_{en}$ [where δ_{en} is given by equation (33), for instance], we find that $\mathrm{Pe}_{ov} \propto \mathrm{Ra}_o^{0.27}$. It would require a Rayleigh number 10^4 times larger, therefore a Péclet number 10 times larger than what we currently have in order to get a fully mixed region, i.e. pure penetration. This is quite large, but may actually be achievable in the not-too-distant future[2] (especially if one were to use a reduced computational domain consisting of a wedge, rather than a full sphere).

ACKNOWLEDGEMENTS

The authors thank C. Guervilly for setting up the two-layered (CZ-RZ) configuration in the PARODY code and for technical and scientific advice. This work was financially supported by National Aeronautics and Space Administration (NASA) Grant No. NNX14AG08G. Simulations were run on the Hyades cluster at the University of California, Santa Cruz, purchased using the National Science Foundation (NSF) grant No. AST-1229745, as well as on the XSEDE Stampede 2 Texas Advanced Computing Center (TACC) at The University of Texas at Austin.

REFERENCES

Ahrens B., Stix M., Thorn M., 1992, A&A, 264, 673
Aubert J., Aurnou J., Wicht J., 2008, Geophys. J. Int., 172, 945
Baraffe I., Pratt J., Goffrey T., Constantino T., Folini D., Popov M. V., Walder R., Viallet M., 2017, ApJ, 845, L6
Böhm-Vitense E., 1958, Z. Astrophys., 46, 108
Brandenburg A., 2016, ApJ, 832, 6
Browning M. K., Brun A. S., Toomre J., 2004, ApJ, 601, 512
Browning M. K., Miesch M. S., Brun A. S., Toomre J., 2006, ApJ, 648, L157
Browning M. K., Brun A. S., Miesch M. S., Toomre J., 2007, Astron. Nachr., 328, 1100
Brummell N. H., Clune T. L., Toomre J., 2002, ApJ, 570, 825
Brun A. S. et al., 2017, ApJ, 836, 192
Brun A. S., Browning M. K., Toomre J., 2005, ApJ, 629, 461
Brun A. S., Miesch M. S., Toomre J., 2011, ApJ, 742, 79
Charbonneau P., MacGregor K. B., 1997, ApJ, 486, 502
Christensen-Dalsgaard J., Gough D. O., Thompson M. J., 1991, ApJ, 378, 413
Christensen-Dalsgaard J., Monteiro M. J. P. F. G., Rempel M., Thompson M. J., 2011, MNRAS, 414, 1158
Christensen-Dalsgaard J., Gough D. O., Knudstrup E., 2018, MNRAS, 477, 3845
Cogan B. C., 1975, ApJ, 201, 637
Couston L.-A., Lecoanet D., Favier B., Le Bars M., 2017, Phys. Rev. Fluids, 2, 094804
Cox J. P., Giuli R. T., 1968, Principles of Stellar Structure. Gordon and Breach, New York
Deardorff J. W., 1966, J. Atmos. Sci., 23, 503
Deardorff J. W., Willis G. E., Lilly D. K., 1969, J. Fluid Mech., 35, 7
Deheuvels S., Brandão I., Silva Aguirre V., Ballot J., Michel E., Cunha M. S., Lebreton Y., Appourchaux T., 2016, A&A, 589, A93
Dormy E., Cardin P., Jault D., 1998, Earth Planet. Sci. Lett., 160, 15
Freytag B., Ludwig H.-G., Steffen M., 1996, A&A, 313, 497
Ghizaru M., Charbonneau P., Smolarkiewicz P. K., 2010, ApJ, 715, L133
Gough D. O., Spiegel E. A., Toomre J., 1975, J. Fluid Mech., 68, 695
Herring J. R., 1963, J. Atmos. Sci., 20, 325
Herwig F., 2000, A&A, 360, 952
Hurlburt N. E., Toomre J., Massaguer J. M., 1986, ApJ, 311, 563
Hurlburt N. E., Toomre J., Massaguer J. M., Zahn J.-P., 1994, ApJ, 421, 245
Käpylä P. J., Rheinhardt M., Brandenburg A., Arlt R., Käpylä M. J., Lagg A., Olspert N., Warnecke J., 2017, ApJ, 845, L23
Kippenhahn R., Weigert A., 1990, Stellar Structure and Evolution. Springer, Berlin

[2]Recall that Ra_o is based on the length-scale r_o rather than the width of the CZ, so the effective Rayleigh number of our simulations is smaller than Ra_o.

Korre L., Brummell N., Garaud P., 2017, Phys. Rev. E, 96, 033104
Latour J., Spiegel E. A., Toomre J., Zahn J.-P., 1976, ApJ, 207, 233
Latour J., Toomre J., Zahn J.-P., 1981, ApJ, 248, 1081
Liu Z. et al., 2014, ApJ, 780, 152
Maeder A., 1975, A&A, 40, 303
Malkus W. V. R., 1960, in Thomas R. N., ed., Proc. IAU Symp. 12, Aerodynamic Phenomena in Stellar Atmospheres. Bologna, Italy
Massaguer J. M., Latour J., Toomre J., Zahn J.-P., 1984, A&A, 140, 1
Miesch M. S., Brun A. S., Toomre J., 2006, ApJ, 641, 618
Monteiro M. J. P. F. G., Thompson M. J., 1998, in Korzennik S., ed., ESA Special Publication Vol. 418, Structure and Dynamics of the Interior of the Sun and Sun-like Stars. ESA, Paris, p. 819
Monteiro M. J. P. F. G., Christensen-Dalsgaard J., Thompson M. J., 1994, A&A, 283, 247
Moore D. R., Weiss N. O., 1973, J. Fluid Mech., 61, 553
Morton B. R., Taylor G., Turner J. S., 1956, Proc. R. Soc. A, 234, 1
Musman S., 1968, J. Fluid Mech., 31, 343
Muthsam H. J., Goeb W., Kupka F., Liebich W., Zoechling J., 1995, A&A, 293, 127
Parker E. N., 1993, ApJ, 408, 707
Paxton B. et al., 2013, ApJS, 208, 4
Paxton B., Bildsten L., Dotter A., Herwig F., Lesaffre P., Timmes F., 2011, ApJS, 192, 3
Pinsonneault M., 1997, ARA&A, 35, 557
Pratt J., Baraffe I., Goffrey T., Constantino T., Viallet M., Popov M. V., Walder R., Folini D., 2017, A&A, 604, A125
Racine É., Charbonneau P., Ghizaru M., Bouchat A., Smolarkiewicz P. K., 2011, ApJ, 735, 46
Rempel M., 2004, ApJ, 607, 1046
Renzini A., 1987, A&A, 188, 49
Roberts P. H., 1966, in Donnelly R. J., Herman R., Prigogine I., eds, Non-Equilibrium Thermodynamics, Variational Techniques, and Stability. Cambridge Univ. Press, Cambridge, p. 125
Rogers T. M., Glatzmaier G. A., 2005, ApJ, 620, 432
Rogers T. M., Glatzmaier G. A., Jones C. A., 2006, ApJ, 653, 765
Saikia E., Singh H. P., Chan K. L., Roxburgh I. W., Srivastava M. P., 2000, ApJ, 529, 402
Schmitt J. H. M. M., Rosner R., Bohn H. U., 1984, ApJ, 282, 316
Shaviv G., Salpeter E. E., 1973, ApJ, 184, 191
Silva Aguirre V., Ballot J., Serenelli A. M., Weiss A., 2011, A&A, 529, A63
Singh H. P., Roxburgh I. W., Chan K. L., 1995, A&A, 295, 703
Singh H. P., Roxburgh I. W., Chan K. L., 1998, A&A, 340, 178
Spiegel E. A., 1963, ApJ, 138, 216
Spiegel E. A., Veronis G., 1960, ApJ, 131, 442
Spite F., Spite M., 1982, A&A, 115, 357
Straus J. M., Blake J. B., Schramm D. N., 1976, ApJ, 204, 481
Strugarek A., Brun A. S., Zahn J.-P., 2011, A&A, 532, A34
Sukhbold T., Woosley S. E., 2014, ApJ, 783, 10
Toomre J., Zahn J.-P., Latour J., Spiegel E. A., 1976, ApJ, 207, 545
Toomre J., Gough D. O., Spiegel E. A., 1977, J. Fluid Mech., 79, 1
Toomre J., Gough D. O., Spiegel E. A., 1982, J. Fluid Mech., 125, 99
Townsend A. A., 1964, Q. J. R. Meteorol. Soc., 90, 248
van Ballegooijen A. A., 1982, A&A, 113, 99
Veronis G., 1963, ApJ, 137, 641
Zahn J.-P., 1991, A&A, 252, 179
Zahn J.-P., Toomre J., Latour J., 1982, Geophys. Astrophys. Fluid Dyn., 22, 159

This paper has been typeset from a TEX/LATEX file prepared by the author.